L-PBF and Heat Treatment of 17-4PH steel

Project title: INSIDE Metal AM
Project Type: Speerpuntcluster-VIS-project
Project duration: 01/04/2018 – 31/12/2020

This project received support from the Strategic Initiative Materials (SIM Flandres) and het Vlaams Agentschap voor Innoveren & Ondernemen (Vlaio).

Project partners: Sirris, CRM, BIL

Document type: project report
Version: v1.0, 26/02/2021
Author: Jeroen Tacq, jeroen.tacq@sirris.be

More information about this project can be found on: https://www.sirris.be/inside-metal-additive-manufacturing

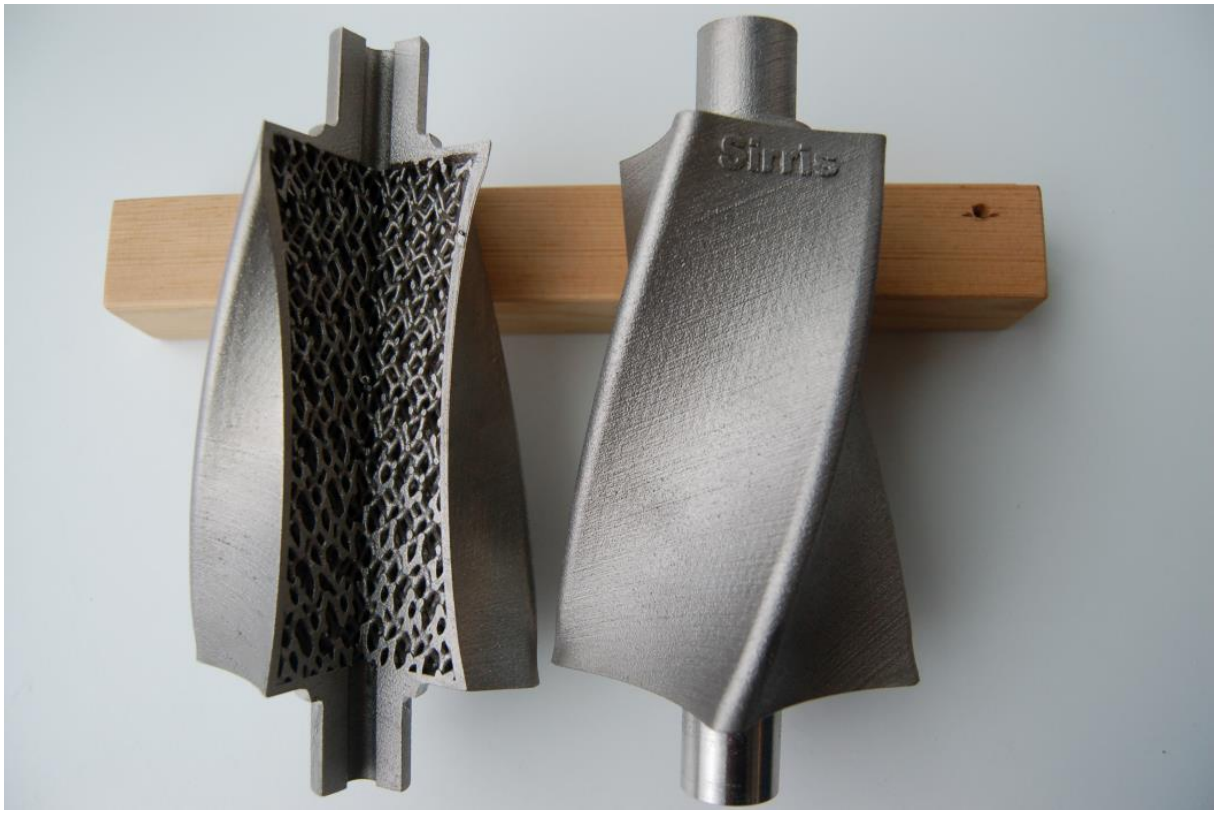

Demonstrator parts printed using 17-4PH steel on an SLM250 machine.

Abbreviations and symbols

MPB	Melt Pool Boundary
R_p	Proof stress/Yield stress
R_m	Ultimate Tensile Strength
ε_m	Elongation at fracture
NNS	Near Net Shape
AB	As-Build
HT	Heat Treatment
LOM	Light Optical Microscopy
SEM	Scanning Electron Microscopy
L-PBF	Laser Powder Bed Fusion

Table Of Content

1 Summary and purpose of the report

In the framework of the INSIDE Metal AM project (2017-2021), a study was undertaken to clarify the process-property-structure relationship in 17-4PH steel manufactured using L-PBF, followed by heat treatment. The report is primarily aimed at readers with an industrial background that are looking for a deeper insight in L-PBF of 17-4PH steel. However, the results are based on an extensive experimental program and are presented in sufficient depth in order to also be of relevance for an academic reader. An industrial reader is advised to start at the end of this report, with the main lessons learned as presented in chapter 7, and look back at previous sections if more information is required. For more information, the reader is welcome to contact the author directly.

The work presented here was done in preparation of printing of demonstrator parts (see cover picture). The purpose of this report is to allow people who are printing 17-4PH themselves, are considering to start printing, or are working with external service providers to learn from our work what are the key elements to consider when using this material.

In chapter 2, a general introduction is given on 17-4PH steel, followed by reference properties for both the conventional and L-PBF steel. Chapter 2 then continues with a short review of the academic literature, providing a quick introduction to the microstructures and properties that can be expected. In chapter 3, the experimental details of the work undertaken are presented. The results from a wide parameter study (including heat treatment) are presented in sections 4.1 to 4.4, focussing on density, porosity, microstructure and tensile properties. The results are discussed in section 4.5. The discussion is presented as the answer to a number of questions that can be answered with the results obtained in the previous sections:

- How important is the anisotropy of the material, and does it change after HT?
- Does the solution annealing treatment influence the properties after HT?
- How do the properties after HT compare to AB, and conventional material?
- Does a change in process parameters from high power and scan speed low power and scan speed influence the properties?
- Does the hardness correlate well to the tensile properties? And can it thus be used as a simple and fast tool for parameter optimization.
- Does the surface condition influence the tensile properties?

For the results of surface post-processing the reader is referred to the complementary information in the document 'Surface finishing of L-PBF and LMD parts' on the project webpage[1]. The main lessons learned from printing of the demonstrator parts are summarised in chapter 6. And, as mentioned above, the main Lessons Learned from the work on process optimisation and heat treatment are summarized in chapter 7. The author of this report welcomes any feedback and questions you might have. Contact info can be found on the cover page of this report.

2 Introduction

2.1 17-4PH Steel

Alloy 17-4PH (UNS S17400, type 630, X5CrNiCuNb16-4) is a chromium-nickel-copper precipitation-hardening martensitic stainless steel with an addition of niobium. 17-4PH combines high strength and hardness with good corrosion resistance. The corrosion resistance of Alloy 17-4PH is comparable to 304 stainless steel in most environments, and is generally superior to the 400 series stainless steels because of low carbon content. A range of properties and hardness can be achieved through modifications of the aging temperature during heat treatment. 17-4PH is magnetic. Alloy 17-4PH can be easily welded and processed by standard shop fabrication practices.

Conventional 17-4PH is used in applications where the combination of moderate corrosion resistance and high strength are required. It is a material of choice in medical, surgical, aerospace and defence products. It should not be used at working temperatures above 300-315°C or for cryogenic service.

[1] https://www.sirris.be/inside-metal-additive-manufacturing

2.2 Reference properties

	SUPPLIER	DENSITY [G/CM³]	YIELD STRESS [MPA]	TENSILE STRENGTH [MPA]	ELONGATION [%]	E-MODULUS [GPA]	HARDNESS
CONDITION A	Conventional (ATI)	7.75	760	1030	8	196	33 HRC
AS-BUILD	SLM Solutions	-	572	832	31	155	221 HV10
	Concept Laser	-	-	-	-	-	-
	3D Systems 17-4PH (A), Z-direction	>99.9%*	830	1100	19		32 HRC
H900	Conventional (ATI)	7.81	1240	1340	10	196	43 HRC
	SLM Solutions	-	-	-	-	-	-
	Concept Laser	-	1250	1350	5		43-46 HRC
	3D Systems 17-4PH (A) , Z-direction	>99.9%*	1260	1380	12		40 HRC
H1150	Conventional (ATI)	7.86	860	1000	10	196	31 HRC
	SLM Solutions	-	-	-	-	-	-
	Concept Laser	-	820	900	13		31-35 HRC
	3D Systems 17-4PH (A) , Z-direction	>99.9%*	1020	1080	16		35 HRC

*With respect to theoretical density of 7.75 g/cm³

	Fe	Cr	Ni	Cu	Mn	Nb + Ta	Si	C	P	S	O
CONVENTIONAL (ATI)	Bal.	15.5	4.5	3.5	0.4	0.3	0.5	0.04	0.02	0.005	-
SLM SOLUTIONS	Bal.	15-17.5	3.0-5.0	3.0-5.0	1	0.15-0.45	1	0.07	0.04	0.03	0.1
CONCEPT LASER	Bal.	15-17.5	3.0-5.0	3.0-5.0	0-1.0	0.15-0.45	0-1.0	0-0.07	0-0.04	0-0.03	
3D SYSTEMS 17-4PH (A)	Bal.	15-17.5	3.0-5.0	3.0-5.0	<1.0	0.15-0.45	<1.0	<0.07	<0.040	<0.03	

2.3 Academic literature

2.3.1 Expected As-Build microstructure

The As-Build microstructure has been reported as consisting of elongated columnar grains, oriented along the build direction. Primary grains can span several melt pool layer thicknesses. The last to solidify interdendritic regions, between the primary dendrites/cells, contain nanoscale NbC-rich precipitates [8]. In [5] grain boundaries in the vicinity of the melt pool were shown to contain smaller columnar grains oriented toward the top centre of the melt pool. Shorter time for cooling (decreased interlayer time) led to coarser columnar grains. This was attributed to the shorter cooling times causing a higher bulk temperature, resulting in lower cooling rates and thus coarser grain sizes. Delta-ferrite stringers in the martensitic matrix, may also be observed along grain boundaries [16].
Various as-build phase compositions for precipitation hardening steels like 17-4PH produced by SLM have been reported, ranging from fully ferritic over a mixture of martensite and (metastable) austenite to fully austenitic. In [8] a dendritic structure containing a substantial fraction of nearly 50% of retained austenite along with body centred cubic/martensite and fine niobium carbides preferentially aligned along interdendritic boundaries is reported. In each case, this is very different from the expected fully martensitic structure for wrought material [2,3,4,5] (with the exception of a small fraction of body centred cubic (BCC) δ-ferrite) that has poor ductility and susceptibility for embrittlement and stress corrosion cracking [8]. Microhardness measurements performed in [5] indicated that a higher amount of retained austenite translates in a lower hardness.
In [8] it is suggested that there could be a strong dependence of material microstructure and phase constitution on process parameters, particularly the presence of a significant fraction of retained austenite. The differences in reported microstructures may also be linked to difficulties in separating the phases. Therefore, a careful investigation with a combination of techniques (EBSD, XRD, SEM) is required [2]. In addition, small variations in steel chemistry and processing can have a pronounced effect on the phase composition [4], which may be particularly important for AM, where the chemistry can change due to preferential vaporisation or changes in starting powder chemistry.
The formation of retained austenite could be caused due to the absorption of nitrogen, an austenite stabilizer, from both powder processing and AM environments, resulting in a decreased martensite transition start temperature, Ms. The results in [12] show that any amount of nitrogen stabilizes the formation of the γ-austenite in L-PBF 17-4PH and causes a decrease of δ-ferrite. These predictions are consistent with observations from [13], where a microstructure consisting mainly of austenite phase (99.3 %) was reported, when nitrogen gas atomized PH17-4 metal powder was used in combination a N_2 environment in the build chamber. The resulting nitrogen content in the manufactured material was 0.17 wt%. In contrast, argon (Ar) atomized PH17-4 powder led to a predominant martensitic microstructure, (87 % martensite). The calculations in [12] assume N contents of up to 0.15wt%.Comparison of elemental analysis of powder, as-build parts and post heat treated parts may shed more light on the influence of chemical composition and/or nitrogen absorption.
Another reason for the increased contents of retained austenite could be the extremely fine sub-grain sizes obtained during AM that again lower the Ms temperature and suppress the martensitic transformation. [8] The microstructure within individual melt pools reveals a dendritic-cellular solidification structure. The found dendrites are oriented predominantly along the build direction, indicating that the general direction of heat flow during solidification is along the build direction. Although dendrites at angles to the build direction are also easily observed, indicating that other effects, such as the direction of the laser scan, play a role in the local heat flow.

2.3.2 Heat treatments proposed and resulting microstructures

17-4PH steel obtains it's high hardness and high strength as a result of precipitation hardening, resulting in the formation of nanoscale, Cu-rich precipitates [11]. In order to allow this strengthening by precipitation, a martensitic microstructure is required [1]. The copper-rich precipitates can be formed within the martensite matrix during the aging process. Conventional 17-4PH steels requires a

solution annealing treatment (typically at around 1050°C) prior to the ageing treatment in order to dissolve any large particles that may have formed and obtain a homogeneous distribution of the Cu atoms in the martensite matrix. For L-PBF manufactured material it has been reported that precipitation does not occur spontaneously in the as-built material and also requires an ageing treatment. Typical proposed ageing temperatures for conventional 17-4PH steel are H900 (482°C) and H1150 (621°C).

Both macro- and microsegregation are known to occur in cast alloys depending on the solidification rate, composition of the alloy, mode of heat conduction, and size of the casting. For the 17-4 steel cast alloy, AMS 5355 recommends a homogenization heat treatment at a temperature of 1150°C for >90 min prior to solutionizing at 1050°C in order to reduce this segregation and achieve a more uniform microstructure and chemistry. [8] However, there is no consensus in the literature whether or not ***solution annealing*** should be applied to L-PBF material prior to the precipitation treatment, or if direct ageing provides better properties. In [8] the temperatures and times of heat treatment were chosen as 650°C and 1050°C for 1 h and 1150°C for 2 h to adhere to the EOS technical specification, wrought solutionizing heat treatment, condition A, and AMS 5355 homogenizing heat treatment, respectively. After solution heat treatment (condition A), the dominant phase in the steel is confirmed to be martensite with the amount of retained austenite reduced to approximately 15% to 20%. Microsegregation was observed along former dendrite directions. In [3] it is reported that solution annealed AM samples have a much finer and more homogeneous microstructure than the as-built sample. This is attributed to oxide inclusions, introduced by the AM process, pinning grain boundaries during heat treatment. Which could be an indication that solution annealing has beneficial effects. In addition, it was reported that because of the homogenizing effect of solution annealing, the interface regions of deposited layers and melt pool boundaries fully vanish. [5], which could further improve the mechanical properties. In the same report direct aging at 482°C for 17-4 PH steel did not lead to age hardening, which was attributed to the dual-phase microstructure (martensite and austenite) present in the as-built SLM parts. It was suggested that solution annealing (Condition A) should be conducted prior to aging (Condition H900). [5]

Ageing of 17-4PH steel leads to the formation of nanoscale Cu rich precipitates. In [2] it was found that over-aging of H1025 and H1150 heat treatments does not lead to an expected strength decrease. This agrees to some extent with the results of [11], where mono-atomic coherent Nb-rich clusters (NbC or NbN) were found at early stage of precipitates (after 1h at 450°C), as well as the formation of Cu clusters in the matrix (fine, angstrom-sized nano-clusters), only after 8 hours do the clusters become nanometre sized particles (<6nm). (Cu rich particles consist mainly of Cu (82at%) and Ni (10 at%). Cu rich precipitates were also identified in [10], which were spherical in shape and had sizes on the order of 100-200nm, with NbC particles of somewhat larger size (200-400nm), but more elongated in shape. High ageing temperatures will produce re-austenitisation, which transforms to untempered martensite upon cooling to room temperature [16].

Austenite that is retained in the material, either in the as-built state or the solution annealed state, can potentially be further transformed into martensite by an additional heat treatment (200-300°C), which relieves the high inner stress, to continue growing the martensite grains. Holding the steel at these temperatures for a longer period of time increases the strength and the toughness of the steel. This is known as tempering, which in more carbon rich steels, is characterized by a transformation of a tetragonal martensite into a cubic martensite and a further transformation to a Fe≈2C phase (ε-carbide, hexagonal). Further heating leads to a transformation of ε- carbide into the intermediate phase Fe3C and might continue to decompose retained austenite into martensite, which can be observed by a dilatation of the material. [12]

2.3.3 Expected properties

In addition to the reference properties given in section 2.2, a few literature results are reported here.

An extensive characterisation of the mechanical properties of L-PBF 17-4PH steel has been undertaken in [5]. The found properties can be summarized as:

- Yield: 800-900MPa (higher for horizontal samples)
- Elongation: 4-6% for vertical, 8-10% for horizontal, lower limit for H900, higher for AB
- Hardness: 300-350 HV0.5 (AB), 400-450 HV0.5 (H900)

The observed anisotropy is explained as follows: "The tensile loading axis is parallel to the build direction for the vertically built samples, whereas it is perpendicular to the build direction for horizontally built ones. Thus, weak interfacial layers for vertically built samples are parallel to cracks, providing easier paths for shear band coalescence and void growth under tensile loading compared to horizontally built samples. As a result, vertically built samples exhibit lower strengths and elongation to failure than horizontally built ones, both for as-built and heat-treated conditions." [5]
In research undertaken by the Fraunhofer Institute [15], tensile strengths of over 1000MPa were observed for the as-build material. With targeted post-treatments (including nitriding), tensile strengths of up to 1200MPa were obtained.

In [8] an as-built hardness of only 258 ± 8 VHN is reported, which is lower than its wrought counterpart. Below, some additional results from the same study are included. The lower hardness of the AB material is explained by the high volume fraction (50%) of austenite phase.

Table III. Labels used for identifying the specimens

Sample details	Label	Hardness (VHN)
AM—as built	AM-AB	258 ± 8
AM—EOS stress-relieving heat treatment	AM-SR	312 ± 17
AM—wrought solutionizing heat treatment	AM-S	318 ± 24
AM—AMS 5355 homogenizing heat treatment	AM-H	288 ± 32
Wrought—as-received	W–AR	322 ± 10
Wrought—solution-treated condition	W-S	299 ± 11

The impact of the presence of retained austenite is further discussed in [8] as: "A two-phase structure consisting of martensite and retained austenite may have both detrimental and beneficial effects on the mechanical and corrosion properties of the alloy. The nature and extent of this effect is dictated by the stability of the FCC phase which is linked to its chemistry. Some retained austenite-containing steels exhibit large elongation to failure due to strain-induced transformation of γ -> α'. Yet, having a softer constituent like austenite in the matrix is harmful for the wear resistance of an alloy. In addition, the volume change associated with the phase transformation increases the propensity for cracking."

2.3.4 Expected influence of process parameters

Without careful setting of process parameters, parts with defects (porosity and unmelted powder particles) can be produced [5], which results in reduced mechanical properties. Gu et al. [6] studied the influence of energy density on microstructure and porosity of 17-4 PH parts made by L-PBF. The authors concluded that energy density may only be a weak indicator of porosity level within L-PBF parts, coupons fabricated using the same optimal energy density level showed significantly different levels of porosity.
Parts built under nitrogen contain more retained austenite compared to parts built under argon [7], possibly linked to lower thermal conductivity of argon compared to nitrogen. In [8] it is mentioned that literature shows that the powder atomization and AM build chamber environments (Ar or N2 gas) have demonstrated significant effects on the amount of retained austenite in L-PBF 17-4PH steel. 17-4 PH steel fabricated using selective laser melting method in Ar/Ar (powder atomization/AM environment), Ar/N2 and N2/Ar atmosphere had a martensitic α', structure, whereas in N2/N2 it was predominantly gamma (FCC/austenite) with 15% of α'.
In [5] it was concluded that parts additively manufactured (via laser) with shorter inter-layer time intervals (for example influenced by size of part and amount of parts on the build plate) possess a coarser austenitic microstructure due to lower cooling rates caused by elevated bulk temperature in

the part, resulting in a lower hardness. The thermal history ultimately affects the part properties in the sense that shorter inter-layer time intervals result in more austenitic steel and thus lower microhardness. However, the increase in austenite is less pronounced for SLM than DED processes. It is further mentioned that higher laser powers or lower scan speeds result in higher energy densities, and lower cooling rates. Conversely, higher cooling rates can be achieved by increasing the scan speed or reducing the laser power. In [12] it is also mentioned that lower laser velocities lead to lower solidification velocity which could be detected with a wider spacing between the dendrites. Note that both energy density and inter-layer time intervals are influential factors in the L-PBF process and each can affect the thermal history and thus final properties of the parts.
In [5] the energy density was changed from 93.3 to 106.7 J/mm3, keeping the inter-layer time intervals almost unchanged. An increase in ultimate tensile strength and elongation to failure was then noticed. However, the change in yield stress was not statistically relevant. The change in tensile strength and elongation seemed to be mostly related to a decrease in amount and size of porosity.

3 Work description

3.1 Printing of cube specimens

Goal:

- ✓ Print parameter optimization for 17-4PH
- ✓ Investigate impact of process parameters on density, hardness and microstructure
- ✓ Investigate impact of heat treatment on hardness and microstructure

The cube specimens (10x10x10mm) were used in the print parameter optimisation step. An SLM250 machine was used to build the samples. Three parameters were varied in the process optimisation: hatch spacing ‘h’ (0.09 – 0.15 mm), scan speed ‘v’ (200 – 2600 mm/s) and laser power ‘P’ (175 – 395 W). The layer thickness ‘d’ was kept constant at 30 µm. Build plate temperature was 100°C. The cubes were printed in various jobs, numbered using the date on which they were printed. This job number is used to identify the cubes in many of the graphs shown in this report. Where necessary, the corresponding process parameters are given.
From the print parameters, the energy density ‘E_d’ was calculated and used as a process characteristic. Although there are indications (for example [9]) that the energy density as calculated according to the formula below may not be the optimal design parameters, in the current application oriented research, we have chosen to work with this parameter because of its simplicity, ease of interpretation and the fact that it a commonly known parameter.

$$E_d = \frac{P}{v\,h\,d}$$

The density and hardness of all cubes was determined and microstructure on selected cubes was investigated. The cubes were also used to investigate the influence of heat treatment on the material hardness.

3.2 Printing of tensile specimens

Goal:

- ✓ Investigate impact of process parameters on tensile properties and anisotropy
- ✓ Investigate impact of heat treatment on tensile properties and anisotropy
- ✓ Investigate impact of surface condition on tensile properties

The tensile specimens were cylindrical in shape according to ISO 6892-1, with a diameter of 5mm and gauge length L_c of 30mm. Tensile test samples were either machined from a block specimen (10x10x55mm) or printed near net shape (NNS).

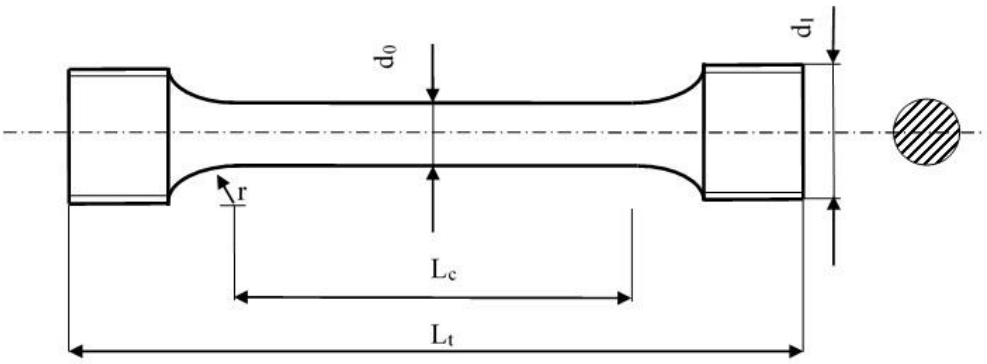

Figure 1: Tensile test sample shape, according to ISO 6892-1.

Tensile properties and the impact of heat treatment on these, was evaluated only for two sets of optimised printer settings:

(1) High power settings: Power: 395 W; Hatch spacing: 0.105 mm; Scan speed: 900 mm/s
(2) Low power settings: Power: 175 W; Hatch spacing: 0.135 mm; Scan speed: 240 mm/s

Layer thickness was 30 µm for all samples. Build plate temperature was 100°C. An SLM250 machine was used to build the samples.

Batch 1: High Power settings

- 3 print jobs of tensile samples, per job 4 block samples in X, Y, and Z direction respectively (10x10x55mm). Each job was used for a different thermal treatment (AB/H900/H1150), from each job, 9 tensile test samples were made.
- Heat treatments including solution heat treatment

Batch 2: Low Power settings (see Figure 2)

- All samples build in vertical direction.
- Half of the samples is near net shape, the other halve are block specimens.
    - Three groups of samples: G1, G2 and G3 (as indicated on the picture). In each group two near net shape (NNS) samples and two block samples.
- H900 samples have not received a solution heat treatment prior to the precipitation hardening.
    - Heat treat samples (H900): G1-A-NNS, G1-A-Block, G2-A-NNS, G2-A-Block, G3-A-NNS, G3-A-Block

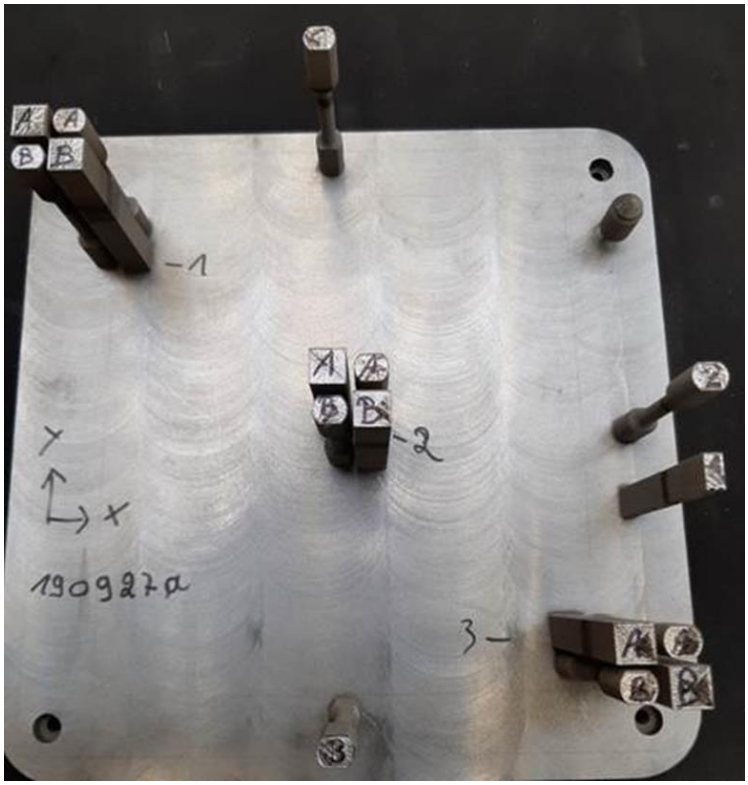

Figure 2: Picture of printed tensile specimens in Batch 2.

3.3 Heat treatments

3.3.1 Annealed condition

Annealing is conducted by heat treating at approximately 1900°F (1040°C) to 1950°F (1065°C) and cooling to room temperature. In this condition, the material possesses a martensitic structure. As a martensitic structure, 17-4PH still possesses a relatively high strength and hardness in the annealed condition.

Conventional 'Condition A' = solution annealed condition (1066°C)

Annealing applied in this project:
Solution annealing, 30 min. at 1045°C, followed by furnace cooling (0.17 K/s in the range from 1000°C to 700°C).

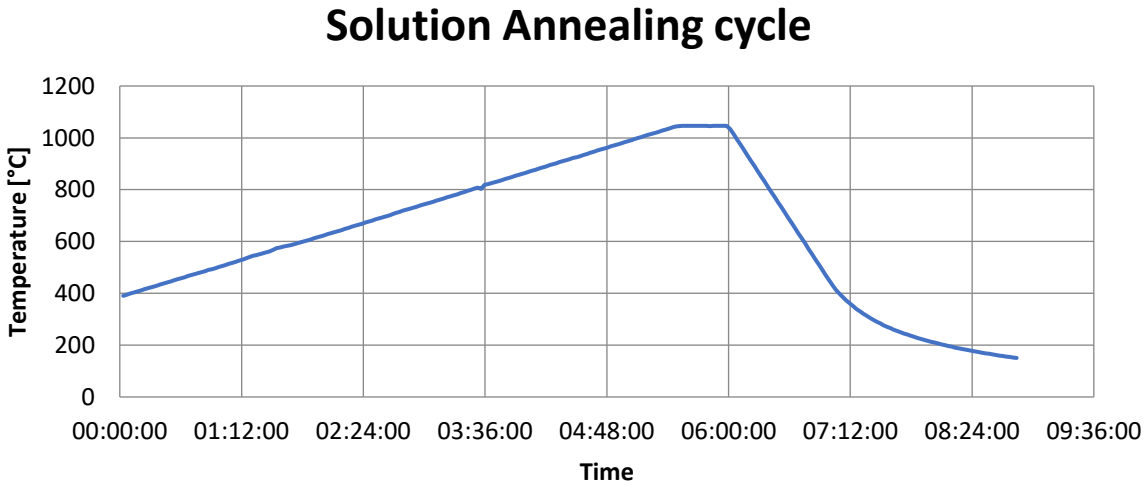

Figure 3: Time-temperature diagram of the annealing treatment applied in this project.

3.3.2 Precipitation hardening

To develop further increase in strength, the annealed material is precipitation hardened by heat treatments at 900°F (482°C). When applied to conventional, wrought 17-4PH steel, these precipitation hardening heat treatments increase ductility and toughness while they harden the material. Heat treatments above 1075°F (579°C) generally result in material softer than material in the annealed condition. Heat treatment in the 900°F (482°C) range produces the highest strength.
The precipitation hardening reaction can be driven past peak strength by heat treating at an excessively high temperature or by excessive time at the precipitation hardening temperature. A less dramatic downward shift in strength results from excessively long precipitation hardening times. H1150 (1150°F, 621°C, for 4 hours), results in a slightly overaged condition, with generally somewhat lower strength and hardness.

H900 performed on the 3D printed parts within this project:
60 min. at 485°C, followed by furnace cooling

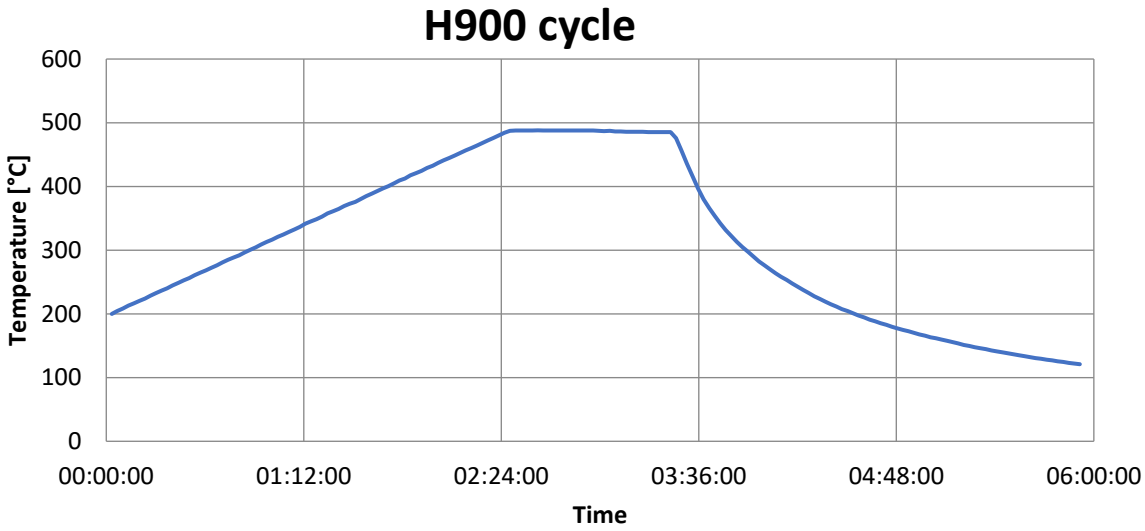

Figure 4: Time-temperature diagram of the H900 treatment applied in this project.

H1150 performed on the 3D printed parts within this project:
4h. at 625-630°C, followed by furnace cooling

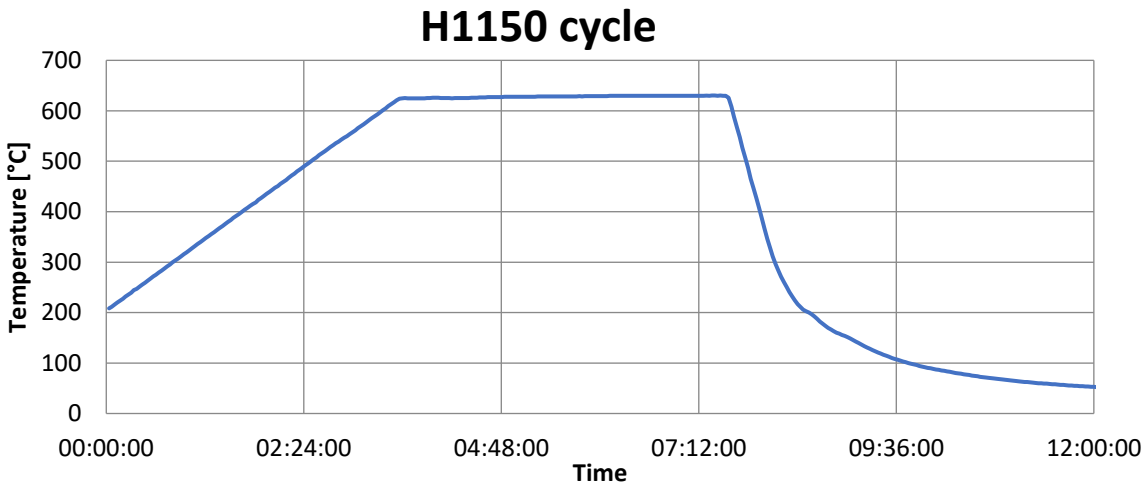

Figure 5: Time-temperature diagram of the H1150 treatment applied in this project.

4 3D printing and heat treatment results

Two types of test samples have been manufactured: cube samples with dimensions of 10x10x10mm, and tensile test samples (see Section 3 Work description).

4.1 Density and porosity

The influence of print process parameters on the density of cube samples was evaluated. In addition, the variation in density of identical cubes on different positions of the build plate was also evaluated to learn more about the process stability. The density of specimens was determined using the Archimedes method.

4.1.1 Influence of process parameters

The influence of the process parameter settings can clearly be seen in the density vs. energy density curve (Figure 6). Starting from low energy densities, the part density quickly increases to 99%. At higher energy densities (> 90 J/mm³) a plateau is reached, with maximum density up to 99.78%. With energy densities increasing beyond 200 J/mm³, the last data points indicate a decline in density. On the plateau itself, there is still quite some variation in the density. The average density for all samples with an energy density between 90 and 200 J/mm³ is 99.24%, with a standard deviation of 0.61%. The outliers indicated by the blue ellipse can be attributed to a dependence of the density on the location on the build plate (see next section). After removal of these outliers, the average density and standard deviation on the plateau are, respectively, 99.38% and 0.16%. No additional correlations between density and individual process parameters could be found in the variations within the plateau. In the next section it is shown that these variations are rather related to position on the build plate.
The process parameters resulting in a high density with least variation over the builds and position on build plate, gave a density of 99.6%. This is still somewhat below the 99.8-99.9% typically requested for commercial applications with steel. With further fine tuning of the settings and machine and process stability optimisation it should be possible to achieve a density of 99.8% or higher, as has been illustrated with some of the highest density samples obtained in this project. Further fine tuning was however not part of the goals of this project.

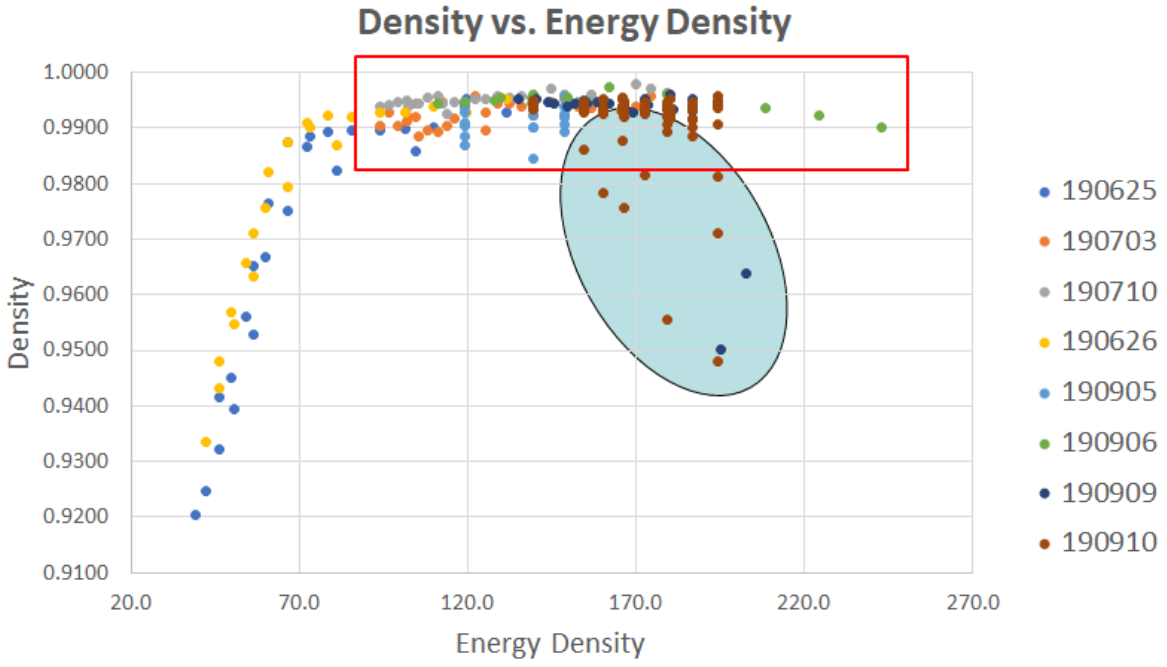

Figure 6: Density of cube samples as a function of energy density (measured using Archimedes method). The numbers in the legend indicate the ID of the print job.

4.1.2 Process stability

As part of the test strategy to learn more about the position dependence of the density, the same matrix of 3x3 cubes was printed 9 times on the build plate, again in a 3x3 matrix. The power setting for all cubes was 175W. In each 3x3 matrix, the hatch spacing was varied from 0.125 to 0.135 mm along the rows and the scan speed varied from 240 to 280 mm/s along the columns. This is illustrated in Figure 7, the measured densities are shown in Table 1. The standard deviation of the density within each small matrix is on average 0.33%. The standard deviation of the density for each set of cubes with identical process parameters but a different position is on average 0.54%. This shows that, within the chosen variation of process parameters, the position dependence is more important than the dependence on process parameters.
In addition, it is clear that the cubes on the left and bottom of the build plate have a lower density. Further investigation showed that this could be attributed to the gas flow in the build chamber. This has been discussed with the machine supplier, and machine upgrades to improve the stability of the gas flow are being implemented.

Figure 7: Test matrix to determine position dependence of the material density, pictures of build plate.

0.9710	0.9902	0.9918	0.9940	0.9938	0.9937	0.9957	0.9916	0.9933
0.9907	0.9934	0.9930	0.9945	0.9939	0.9940	0.9941	0.9933	0.9932
0.9947	0.9953	0.9936	0.9934	0.9926	0.9948	0.9943	0.9948	0.9945
0.9814	0.9914	0.9927	0.9936	0.9936	0.9934	0.9946	0.9948	0.9951
0.9894	0.9928	0.9955	0.9933	0.9933	0.9938	0.9934	0.9948	0.9952
0.9930	0.9932	0.9938	0.9930	0.9933	0.9934	0.9943	0.9932	0.9942
0.9479	0.9884	0.9918	0.9907	0.9934	0.9923	0.9944	0.9938	0.9934
0.9556	0.9814	0.9876	0.9919	0.9924	0.9935	0.9923	0.9935	0.9939
0.9755	0.9784	0.9861	0.9919	0.9932	0.9927	0.9934	0.9936	0.9946

Table 1: Measured densities of cubes printed to determine position dependence of the material density.

4.1.3 Conclusion and selection of print parameters

Two process parameter settings were selected that resulted in an acceptably high density and gave the highest stability, both in terms of position dependence and repeatability between build jobs:

- High power setting: 395W power, 900mm/s scan speed, 0.105mm hatch spacing, 140 J/mm³ energy density
- Low power setting: 175 W power, 240 mm/s scan speed, 0.135 mm hatch spacing, 180 J/mm³ energy density

This selection of process parameter sets also indicates that the energy density, which is different for both sets, is not the only governing parameter, which confirms the observations in [6]. Nevertheless, the energy density can be used to determine a subset of parameter space within which the highest material densities can be found and where further optimisation should focus on. Performing a broad scan of process parameters in a first step makes it possible to quickly find the parameter space in which to operate.

As a reference, in [8] a Nd:YAG laser operating at a power of 195 W was scanned at a speed of 1000 mm/s on a pre-laid powder bed to form a striped scan pattern of a 0.1-mm stripe in raster separation. Laser parameters were optimized to achieve a layer thickness of 20 lm. Volume build and energy densities were maintained at 2 mm3/s and 97.5 J/mm2, respectively.

4.2 Hardness

Next to optimising for density, one might also want to optimise for material properties. This requires that a link exists between the measurable material properties and the process parameters. As it is impractical to print tensile samples for the huge number of possible combinations of process parameters, within this project we have evaluated if the hardness can be used as a quick to measure indication for the mechanical properties. Vickers hardness was measured, using 10kg load. In this section, the observed variations in hardness are discussed and their link to process parameters and heat treatment evaluated.
If the hardness is to be used as an indicator for the mechanical properties, it is important that the hardness is somehow correlated to the tensile properties (which are typically the properties of interest). This is discussed in section 4.5.

4.2.1 Influence of process parameters on hardness in as-build state

Results presented here were obtained from the cube specimens described in section 3.1.

- Due to variations related to position on the build plate (see section 4.1.2) it is difficult to find very strong correlations between hardness and process parameters. Although there seems to be an impact of energy density, as illustrated in Figure 8. It can also be seen that the AB hardness is slightly higher than the hardness indicated in data sheets.

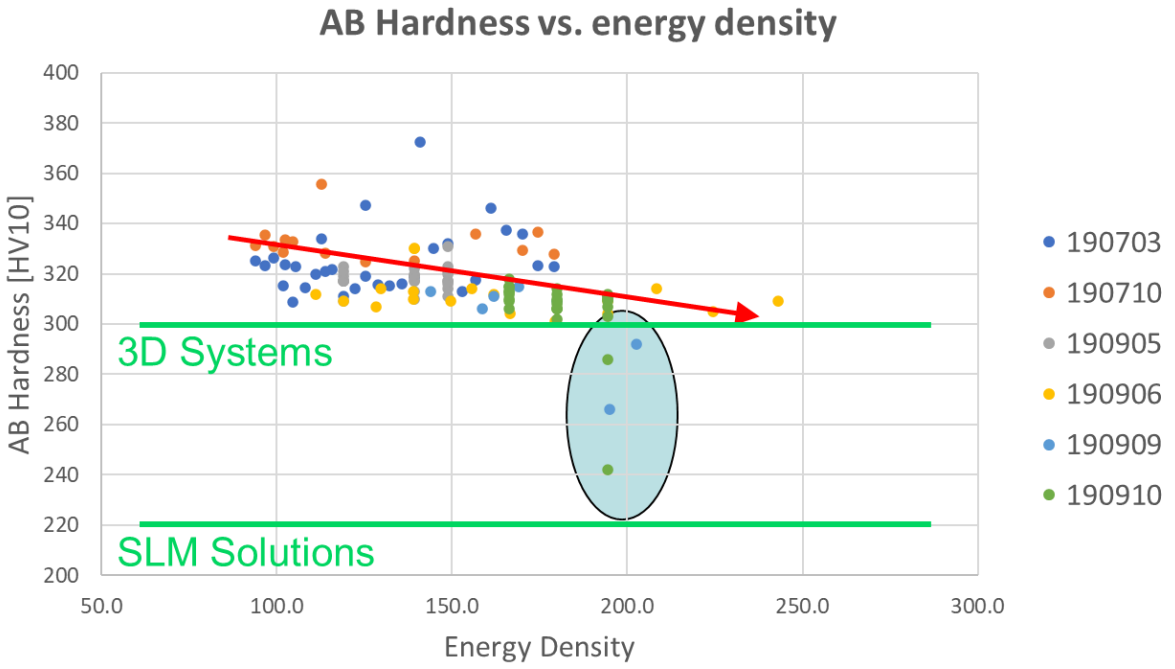

Figure 8: AB Hardness, measured on cube specimens, as a function of Energy Density. The reference values indicated in green are taken from the powder data sheets of the respective machine producers. The outliers indicated with the oval are related to an abnormally low density.

- As shown in Figure 9, there is a strong correlation between hardness and density at densities below 99%. However, at higher densities, there is an additional variation in hardness which is not correlated to the density, as indicated using the two ovals. The correlation between hardness and density should therefore only be used when comparing similar types of samples (similar print parameters and HT).

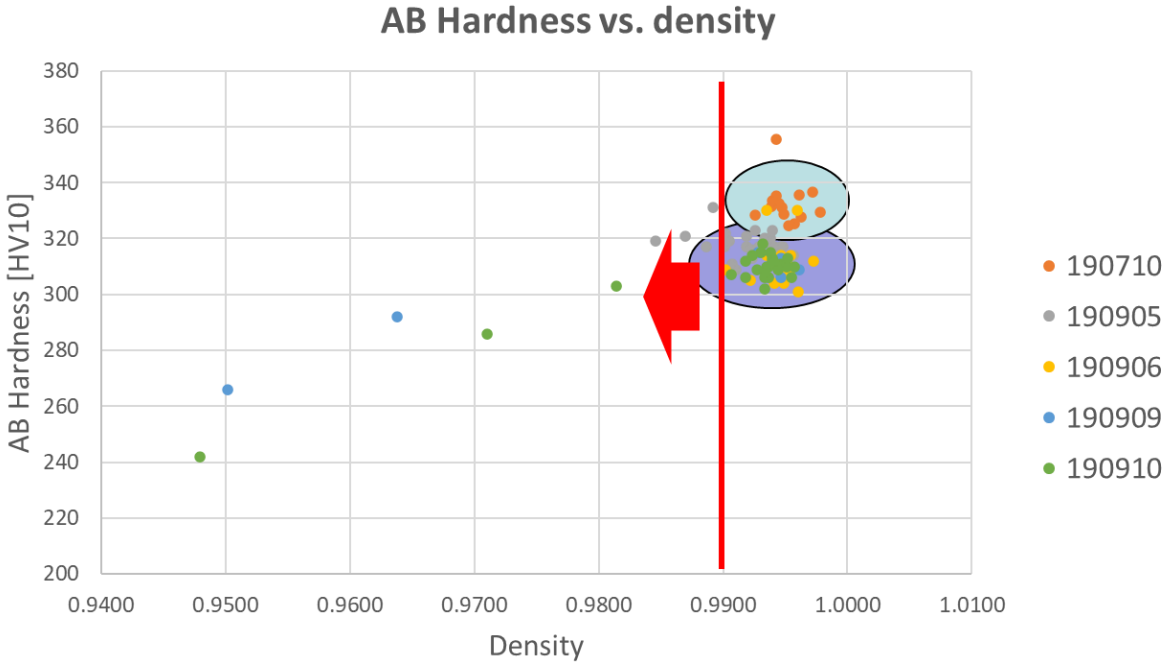

Figure 9: AB Hardness as a function of the density of the cubes (Archimedes method). The vertical red line indicates the start of the plateau identified in section 4.1.1.

- The clustering indicated by the two ovals in Figure 9 is linked to the laser power and scan speed. The measurement results in the high hardness cluster are obtained on cubes printed with higher power and scan speed (range: power 355-395W; scan speed 700-1200mm/s), while the low hardness cluster is obtained on cubes with lower power and scan speed (range: power 175W; scan speed 200-350mm/s). The hardness results averaged over these clusters is given in Table 2. The hardness variations within each cluster were too small to find trends with respect to the range of process parameter variations within the clusters.

	High Power	Low Power
Average AB Hardness	324	308
St. Dev. on total AB population	10.87	12.75

Table 2: AB hardness as a function of print parameters.

4.2.2 Influence of heat treatment

Results presented here were obtained from the cube specimens described in section 3.1.

- A clear difference in hardness between the two types of precipitation hardening treatments (H1150 vs. H900) has been observed. A number of printed cubes were cut in halve, with one halve given H900 and the other a H1150 treatment. Both halves first underwent a solution annealing step. The cubes were printed with parameters in the range: Power, 365-385W; Scan speed, 800-1100mm/s; Hatch spacing 0.105mm. A total of 10 cubes was tested. The hardness results shown in Table 3 clearly illustrate that a H900 precipitation treatment results in a significantly higher hardness, which is as expected.

	H900	H1150
Av.	411	325
St. Dev.	5.33	3.51

Table 3: Hardness as a function of precipitation heat treatment type (H900 vs. H1150).

- In addition, there is also a difference in hardness after H900 treatment, depending on whether or not solution annealing was applied as a first step. Two clusters are observed in Figure 10, with the higher hardness belonging to samples that have not been solution annealed and the lower hardness belonging to samples that were solution annealed prior to the H900 treatment. These observations clearly show that both the solution annealed and non-solution annealed material have a large potential for precipitation hardening, which is in direct contradiction to the results from [5], see section 2.3.2. It also shows that the non-solution annealed material has a somewhat higher precipitation hardening effect, irrespective of the used process parameters.

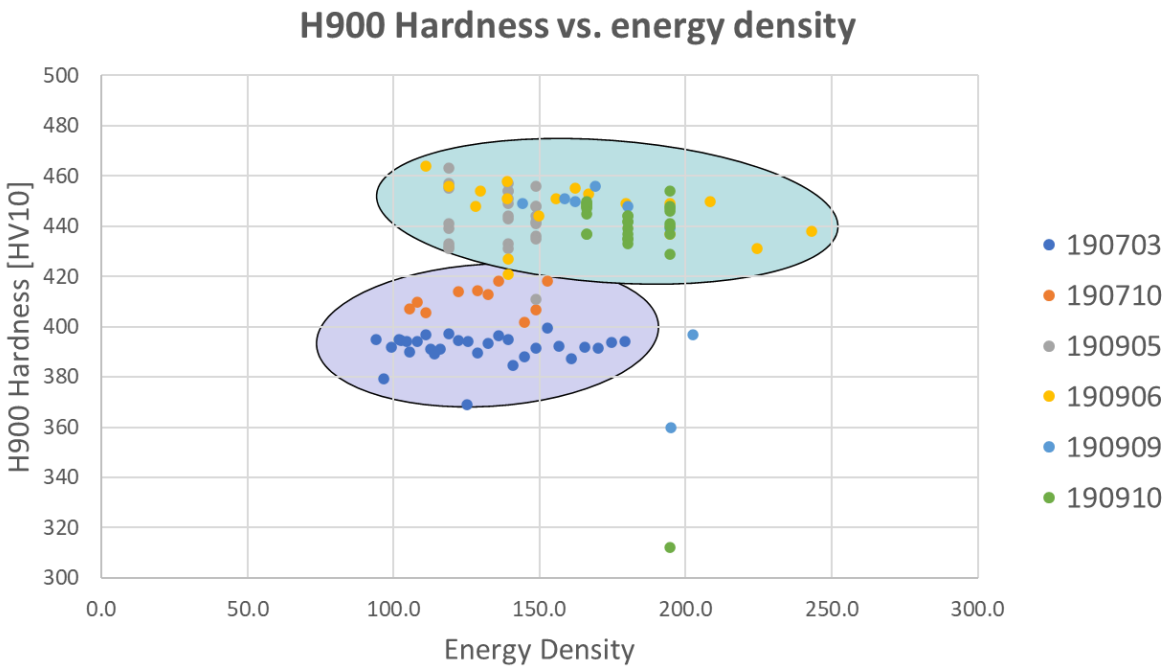

Figure 10: Hardness after H900 heat treatment, as a function of energy density. Two clusters are observed, indicated with the coloured ovals.

- Figure 10 and the results in Table 3 also show that the choice of heat treatment has a dominant effect on the final hardness as compared to the effect of the print parameters. No correlation study between AB hardness and hardness after heat treatment has been performed over a wide range of process parameters. It was therefore impossible to determine whether differences in AB hardness persist after heat treatment. Observations of the microstructure illustrate that the microstructure remains largely unchanged if no solution annealing is performed. In this case, a correlation between AB hardness and hardness after HT can be expected. On the other hand, applying a solution annealing step completely removes the AB microstructure. In this case, no correlation is expected.

4.2.3 Hardness measured on tensile samples

The hardness was also measured on the ends of the printed and tested tensile samples. The densities of the sample ends was measured and found to be in the range of 98.2-98.9%. The measured hardness value are shown in Table 4. Samples from Batch 1 were printed with high power settings, batch 2 samples with low power settings. The H900 HT applied to batch 2 did not include a solution annealing step.

Although the density of the samples is somewhat lower and the number of samples is quite limited the conclusions drawn based on the cube specimens are confirmed:

- H1150 results in a lower hardness as compared to H900.
- Not performing a solution annealing step prior to H900 treatment increases the hardness (although only very slightly here, with significant variations in density making it difficult to draw clear conclusions.)
- The low power settings result in a lower AB hardness.

		AB	H900	H1150
Batch 1	Av. HV10	342	417	306
	St. Dev.	6.34	0.47	14.99
Batch 2	Av. HV10	302	422	-
	St. Dev.	1.50	11.50	-

Table 4: Hardness measured on ends of tensile samples. Averages were determined from 2-3 tensile test specimens each, with 3 measurements done on each end.

4.2.4 Overall conclusion

1. Only weak correlation between print parameters and AB hardness is observed.
2. It is however clear that lowering the laser power and scan speed slightly reduce the AB hardness.
3. For similar samples (similar print parameters and heat treatment), the hardness is correlated to the material density, especially at lower densities (<99%).
4. The choice of heat treatment has a major impact on the hardness.
    a. H900 results in a much higher hardness than H1150
    b. Not performing a solution annealing step results in a higher hardness after subsequent H900 treatment.

Overall, the effect of the type of HT on hardness is much larger than the choice of print parameters. Because in practical applications printed 17-4PH almost always needs to be heat treated to obtain the required material properties, ***hardness is not a good tool for process parameter optimisation. It is advised to optimise for density first and build speed second.***

4.3 Microstructure

The microstructure of a number of selected samples has been investigated using Light Optical Microscopy (LOM) and Scanning Electron Microscopy (SEM). All samples were ground and polished to mirror finish using 1µm diamond paste as a last step. Samples were first investigated prior to etching to identify porosity. Samples were etched using Kallings 2 reagent (20-40s) to reveal the microstructure.

4.3.1 Porosity (non-etched samples)

Below two images are shown to illustrate the comparison between low density samples and the high density (plateau) observed in Figure 6.

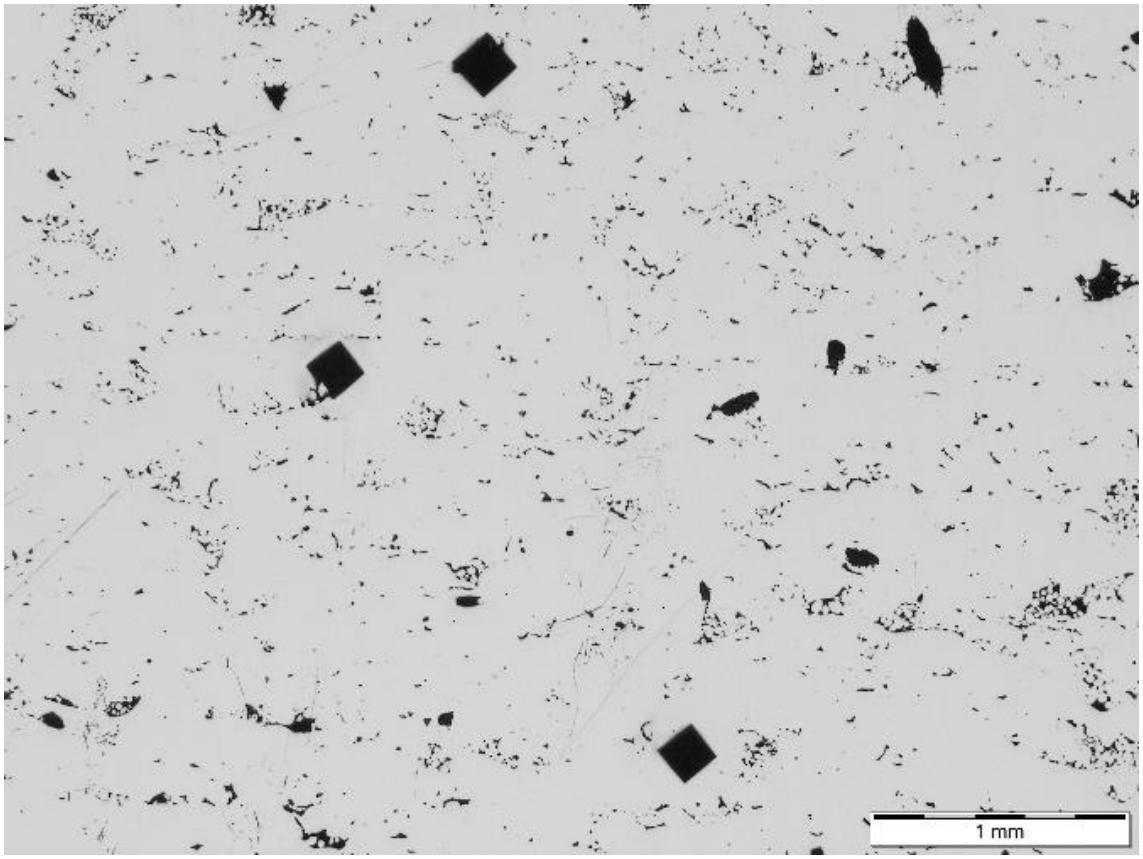

Figure 11: Illustration of a sample with extremely low density. Sample 190625-24, Density: 92.5% (Archimedes method).

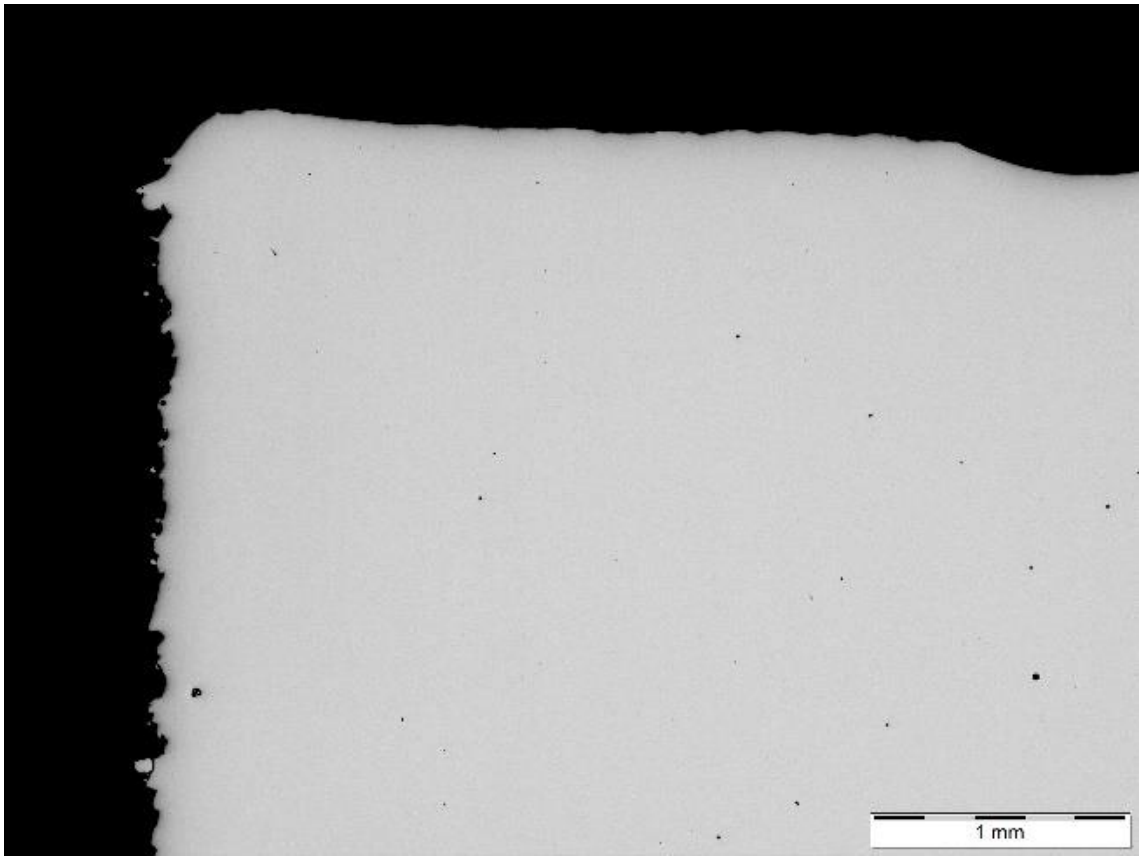

Figure 12: Illustration of a higher density sample. Sample: 190703-5, Density: 99.6% (Archimedes method).

4.3.2 As-build microstructure

The as-build microstructure has been revealed by etching on cross sections made in a plane parallel to the build direction. The microstructure of the samples printed with high power settings exhibits a very regular, columnar grain structure, indicative for a stable growth of the columns (Figure 13). From Figure 14 it can be clearly observed that the columnar grains grow across the MPBs, which is also reported in [8]. A wrought 17-4PH steel typically has a fully martensitic microstructure. Etching with Kallings 2 reagent here clearly reveals the presence of a large amount of retained austenite (white, non-etching phase), next to the martensitic grains (grey etching phase). Small amounts of delta ferrite stringers have also been found, as indicated in Figure 15. The strong directionally of the microstructure can explain the observed anisotropy of the as-build tensile properties, as discussed in section 4.5.1.
It should be remarked that the different phases are not straight forward to identify when comparing to conventional reference microstructures (see Appendix A). In addition, a lot of academic literature is focused on SEM analysis of microstructure and XRD to identify phases. The latter however, doesn't allow to make a clear distinction between martensite and ferrite.

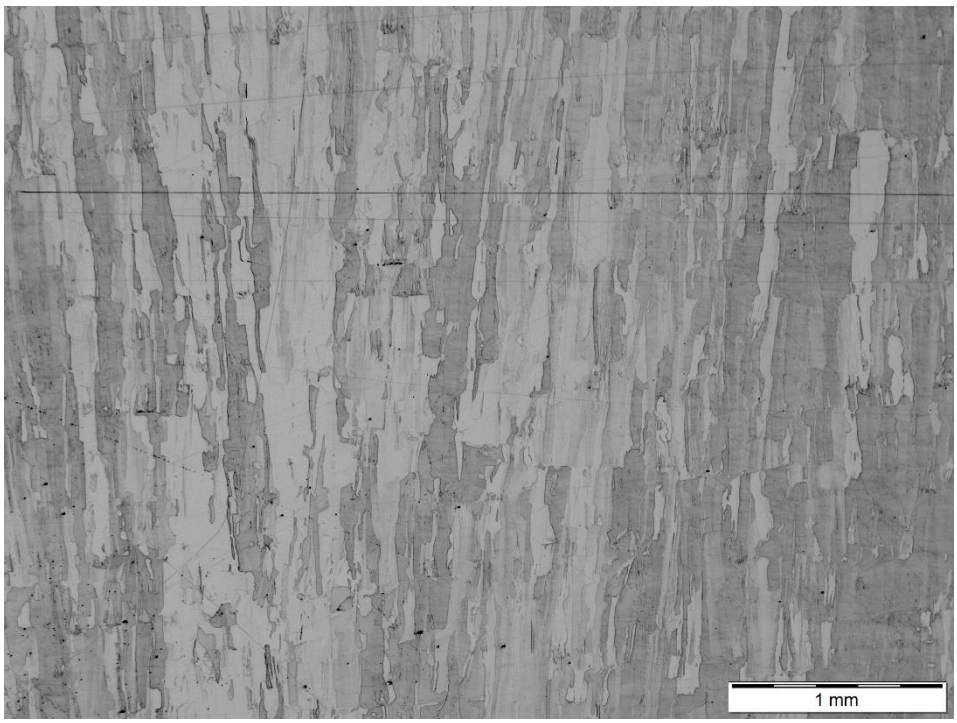

Figure 13: AB microstructure of a sample printed with high power settings, 25x magnification.

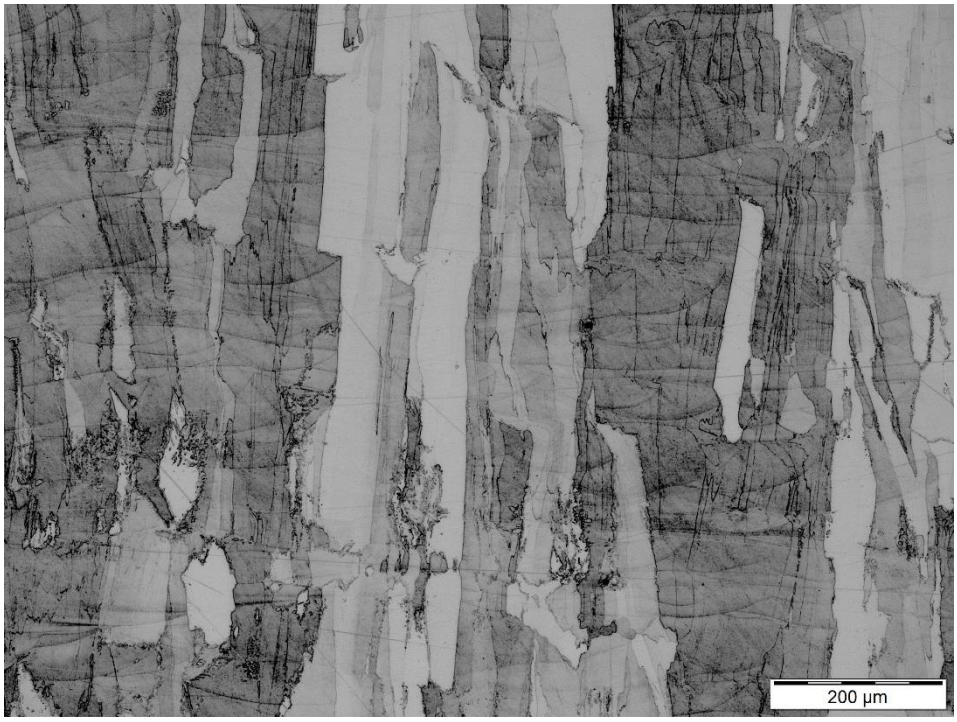

Figure 14: AB microstructure of a sample printed with high power settings, 100x magnification.

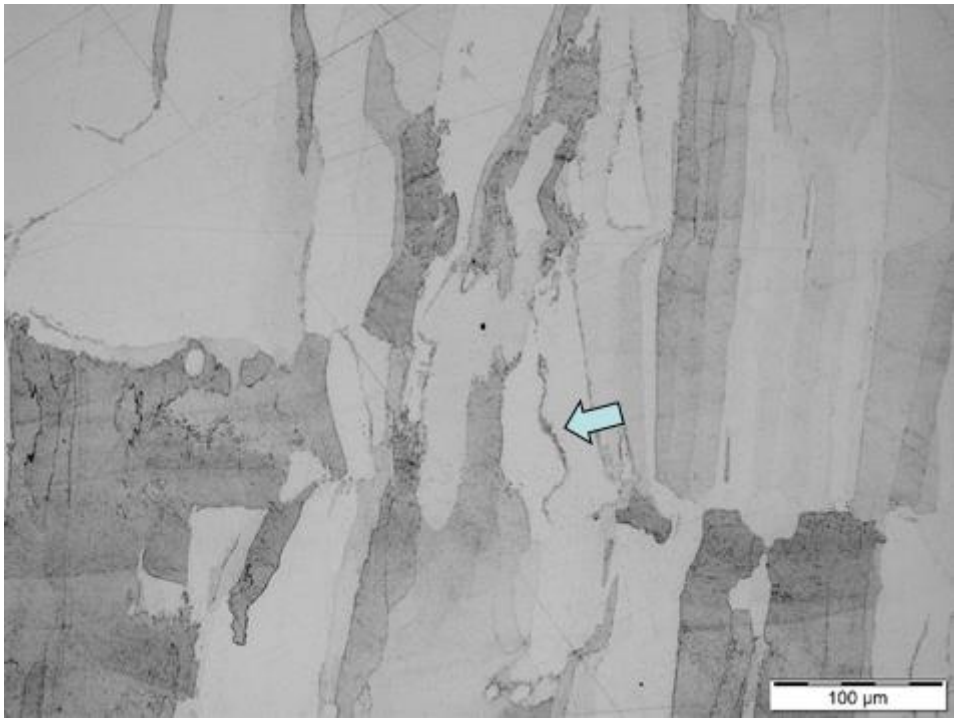

Figure 15: AB microstructure of a sample printed with high power settings, 200x magnification. Delta ferrite stringer indicated with arrow.

The samples printed with low power settings have a much more irregular microstructure (Figure 16), although it is still indicative of columnar growth. This indicates that the columnar growth is less stable at the lower power and scan speed used. The results in [12] support this observation. From fig. 6 in [12], (c vs. d), one might observe that a scan speed of 0.4 mm/sec also leads to a less stable grow of the austenite in comparison to a scan speed of 1mm/sec. Although it must be mentioned that both the process conditions and chemical composition may deviate from the current test results, these observations and scan speeds match well with the current results.

When comparing Figure 16 to Figure 13, one could also conclude that the amount of retained austenite (white, non-etching phase) in the sample printed with low power settings is also higher.

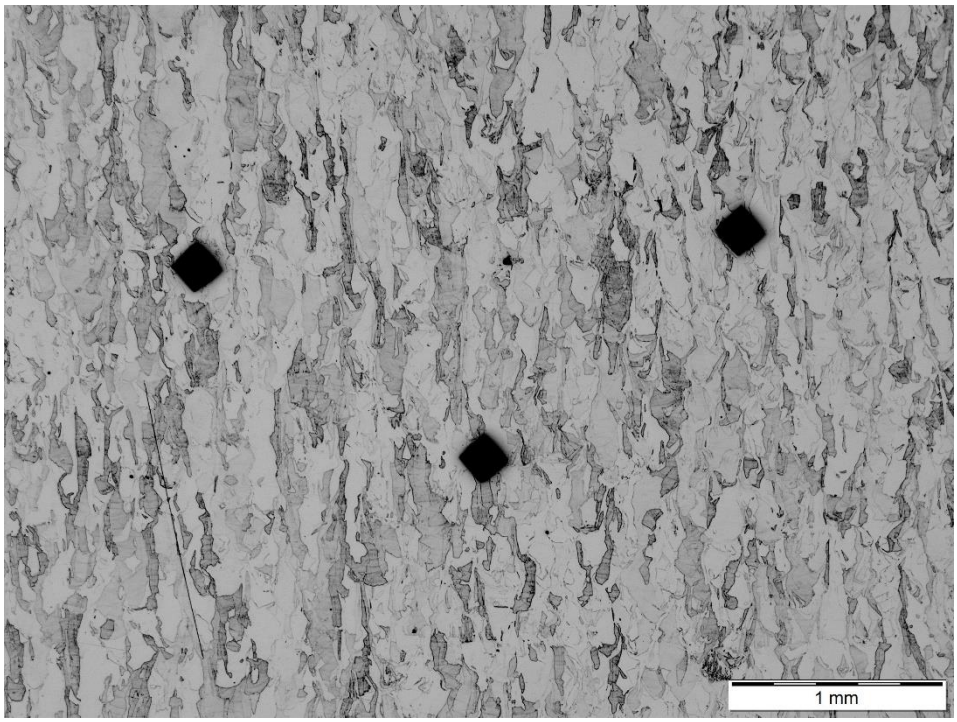

Figure 16: AB microstructure of a sample printed with low power settings, 25x magnification.

A closer examination using SEM clearly reveals that the phase at the grain boundaries is etched deeper than the surrounding material, this agrees with the conclusion that these are delta ferrite stringers (Figure 17). In addition, a very fine subgrain structure is revealed (Figure 18). This is reported in literature as well, for example in [8] where it is mentioned that the microstructure within individual melt pools reveals a dendritic-cellular solidification structure.

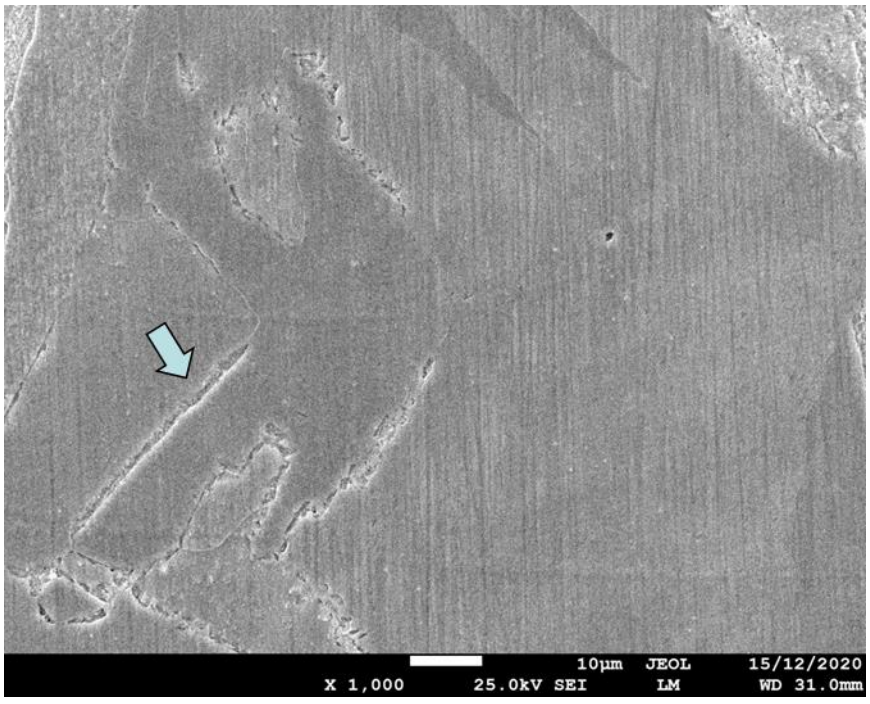

Figure 17: AB microstructure of a sample with low power settings, SEM micrograph. Arrow indicates the presence of a delta ferrite stringer.

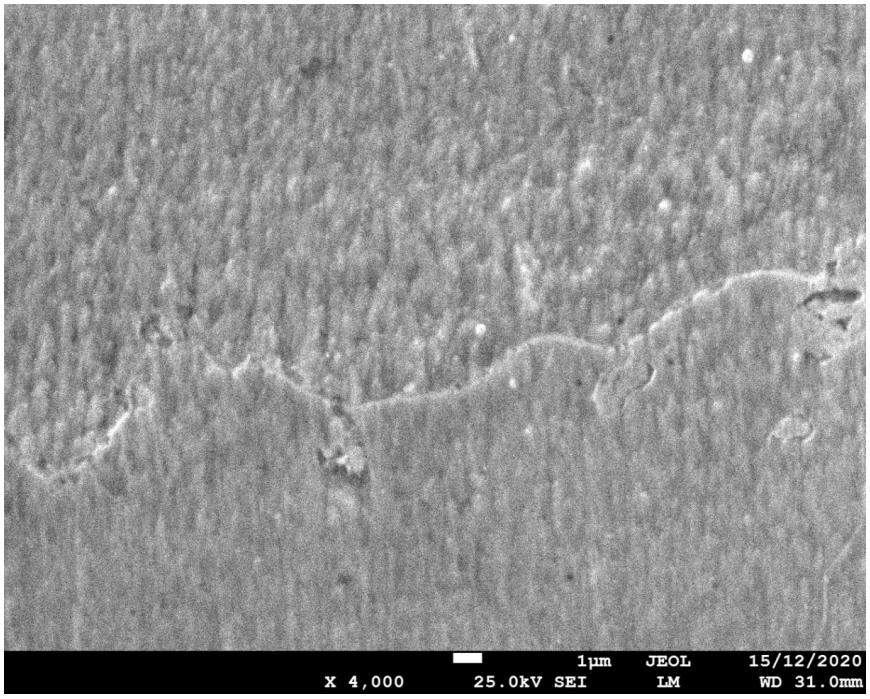

Figure 18: AB microstructure of a sample with low power settings, SEM micrograph. The image reveals the very fine subgrain structure in the material.

4.3.3 Microstructure after heat treatment

Only the microstructure of samples that were given an H900 treatment were investigated, no microstructures of H1150 samples were studied. Prior to looking at the observed microstructures, it should be remarked that precipitation hardening results from the formation of nanoscale precipitates with a high copper content [11],[14]. These nanoscale precipitates are not observable by the LOM and SEM used in this study. However, the hardness results indicate that the precipitation hardening clearly occurs for both the solution annealed material and the non-solution annealed material.

Without solution annealing

If no solution annealing treatment is applied, the observed microstructure is unchanged from the as-build state and still consists of highly elongated grains along the the z-direction, with the presence of some delta ferrite stringers. Even the very fine subgrain structure is retained.

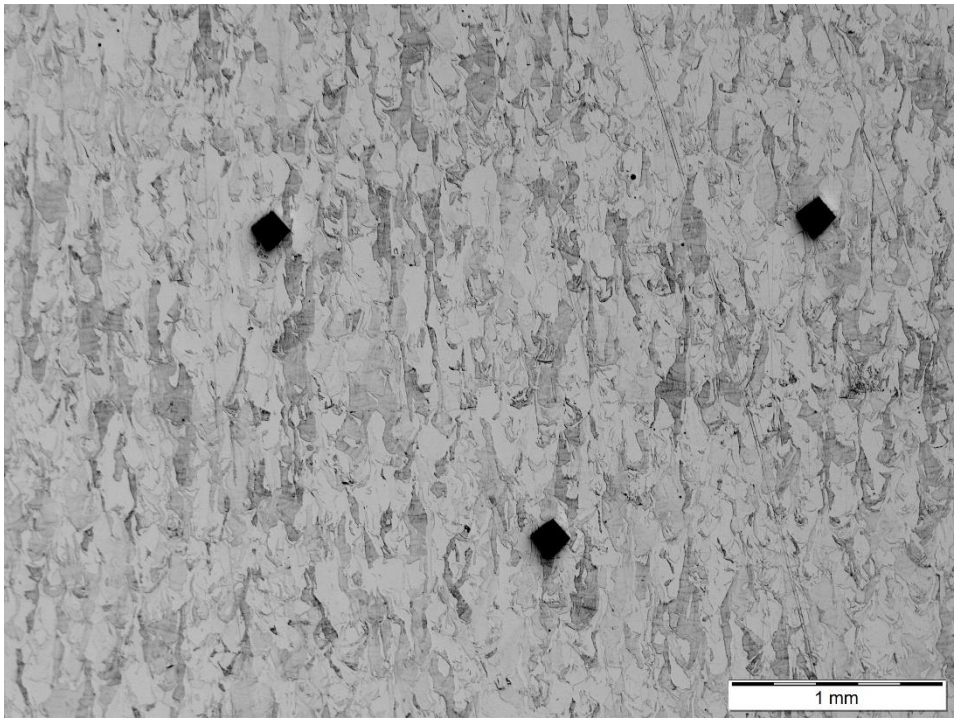

Figure 19: Microstructure of a sample printed with low power settings, after H900 treatment, without solution annealing. x25 magnification.

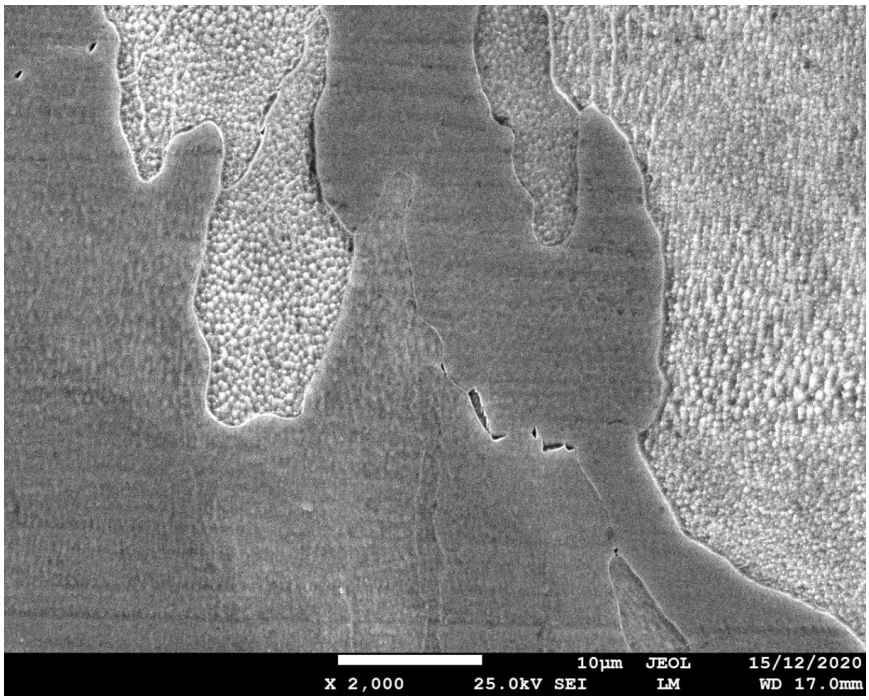

Figure 20: Microstructure of a sample printed with low power settings, after H900 treatment, without solution annealing. SEM micrograph, revealing a very fine subgrain structure.

With solution annealing

After solution annealing followed by a H900 treatment, the microstructure no longer consists of columnar grains. The entire sample now consists of tempered martensite. The grain size has also been reduced as compared to the as-build and non-solution annealed samples. In [3] it is reported that solution HT AM samples have a much finer and more homogeneous microstructure than the as-built sample. This is attributed to oxide inclusions, introduced by the AM process, pinning grain boundaries during heat treatment. Because of the homogenizing effect of solution annealing, the interface regions of deposited layers and melt pool boundaries fully vanish. [5]

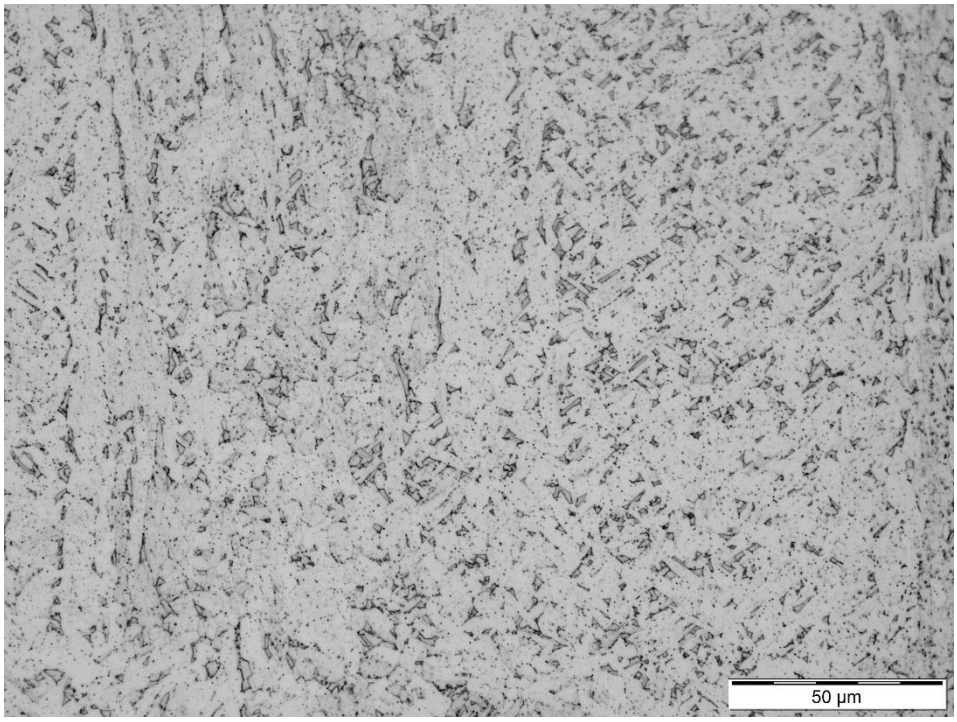

Figure 21: Microstructure of a sample printed with high power settings, after solution annealing and H900 treatment. x500 magnification.

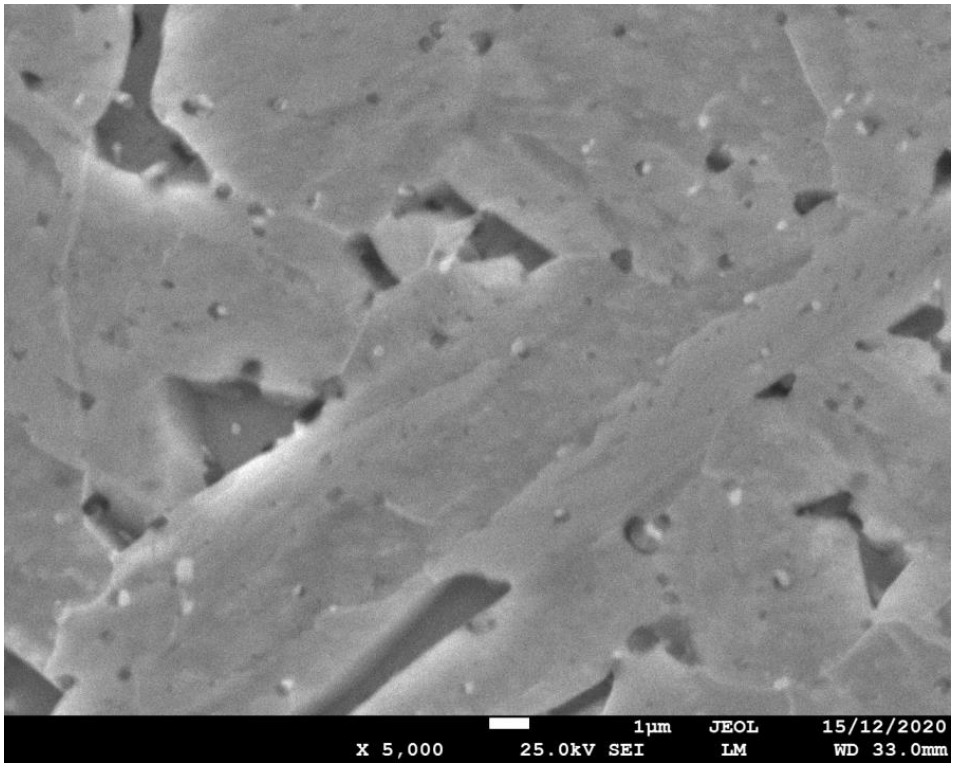

Figure 22: SEM micrograph of the same sample from Figure 21.

4.3.4 Conclusions

There is a significant amount of retained austenite present in the as-build material. The used 17-4PH powder was atomised under N_2 atmosphere, but printed under Ar atmosphere. The maximum N content of the powder is indicated as 0.1wt%. In literature it is indicated that the presence of nitrogen in the material could be responsible for the occurrence of high fractions of retained austenite (see

sections 2.3.1 and 2.3.4), although the printing atmosphere is expected to also have a large influence. Nevertheless, 0.1wt% is on the limit of what is indicated in literature as nitrogen contents that can result in increased amounts of retained austenite, therefore an effect of the atomisation environment cannot be excluded. Another possible reason for the high amounts of retained austenite, mentioned in [8] is the extremely fine sub-grain sizes obtained during AM that again lower the Ms temperature and suppress the martensitic transformation. A similar fine sub-grain structure was also observed here.

Additional conclusions:

- The as-build material exhibits a columnar primary grain microstructure, with the columns being more stable at higher power and scan speed.
- The as-build material exhibits a very fine cellular sub-grain structure.
- After H900 treatment, without solution annealing, the observed microstructure is unchanged.
- After H900 treatment, with solution annealing, the as-build microstructure is completely erased, resulting in a microstructure of tempered martensite.

4.4 Tensile properties

Tensile tests have been performed on two types of specimens, as described in section 3.2. The results of these tensile tests are summarised here and discussed in relation to the other results in section 4.5. Where necessary, the tensile test curves are shown in section 4.5 to support the discussion.

4.4.1 Batch 1 – High Power print settings, solution annealing in HT

		Yield Stress $Rp_{0.2}$ [MPa]	*Tensile strength Rm [MPa]*	*Elongation [%]*	*Hardness [HV]*	*Density [%]*
AB	**X-Y**	782±15	903±64	12.9±4.2		
	Z	727±20	988±44	15.7±0.5	342±6.3	98.26±0.06
H900	**X-Y**	1148±20	1251±52	7.7±3.1		
	Z	1160±4	1265±25	7.5±3.5	417±0.5	98.46±0.13
H1150	**X-Y**	656±18	993±8	15.9±1.4		
	Z	978±2	978±2	16.2±1.4	306±15	98.70±0.25

Table 5: Results tensile tests on Batch 1 samples. (High power and scan speed settings. Solution annealing applied in the heat treatment step.)

4.4.2 Batch 2 – Low Power print settings, no solution annealing in HT

Only tensile tests in Z-direction have been performed.

	Surface condition	*Yield Stress $Rp_{0.2}$ [MPa]*	*Tensile strength Rm [MPa]*	*Elongation [%]*	*Hardness [HV]*	*Density [%]*
AB	**AB**	615±17	874±8	10±7	-	-
	Machined	788±20	888±21	9±2	302±2	-
H900	**AB**[(1)]	948[(1)]	1058[(1)]	-	439±7	98.69
	Machined	974±51	1063±20	3.95[(2)]	422±12	-

Table 6: Results tensile tests on Batch 2 samples. (Low power and scan speed settings. No Solution annealing applied in the heat treatment step.) [(1)]Only one of three samples did not fail early. Other samples failed at a tensile strength of approx. 300MPa, no yield stress could be determine. [(2)]Based on two measurements (4.0 and 3.9), third samples failed outside the strain gauge.

4.5 Discussion: Process-microstructure-properties relationships

4.5.1 How important is the anisotropy of the material, and does it change after HT?

- Literature indicates that vertically build samples have a lower strengths and elongation as compare to horizontally build samples. The reason indicated for this, is that weak interfacial layers (between the build layers, i.e. melt pool boundaries) are perpendicular to the loading direction and parallel to the direction of crack growth. The experimental results from samples collected in the current study do not fully support this view. *The yield strength of as-build samples is indeed somewhat lower in the vertical direction (-65MPa), but the tensile strength is higher (+85MPa), as well as the elongation (+3%) and reduction in area (+25%).* The material data sheets from 3DS also indicate a higher elongation in the Z-direction (although only information is given for XY properties after heat treatment). A possible explanation for the higher elongation (and tensile strength) in the Z-direction could be that it is not the interlayer interfaces that determine the moment of ductile fracture, but the grain boundaries. The microstructure reveals long, columnar grains along the Z-direction that cross multiple melt pool boundaries. These 'fibre like' grains are likely to allow more deformation along their axis as compared to a direction perpendicular to their axis.
  The observation that 0.2% proof (yield) stress is lower, indicates that plastic deformation does occur earlier in the vertical samples. From the load-strain curves, it can be seen that the yielding is very gradual (Figure 24). This could mean that, although the grain boundaries govern the fracture behaviour, that it is the MPBs that govern the onset of plastic deformation and are indeed weaker from that respect (different cellular structure?), but that there is a large spread in 'strength' of the MPBs.
- *The more gradual transition from elastic to plastic behaviour in the as-build sample in the Z-direction* (see stress-strain curves below) results in an apparently higher amount of strain hardening (Rm-Rp), and is to be interpreted as a large strain interval over which micro-plastic deformation is occurring. After solution annealing this gradual transition is no longer observed.
- Overall, the difference in properties between the X and Y directions is negligible.

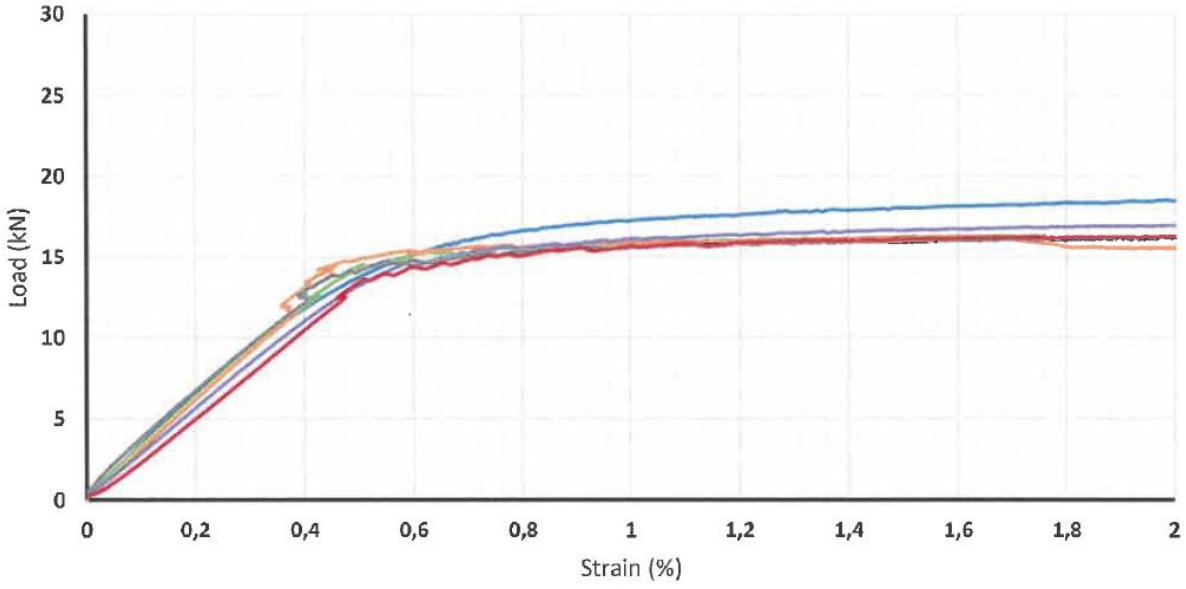

Figure 23: As-build Load-Strain curve, horizontal direction.

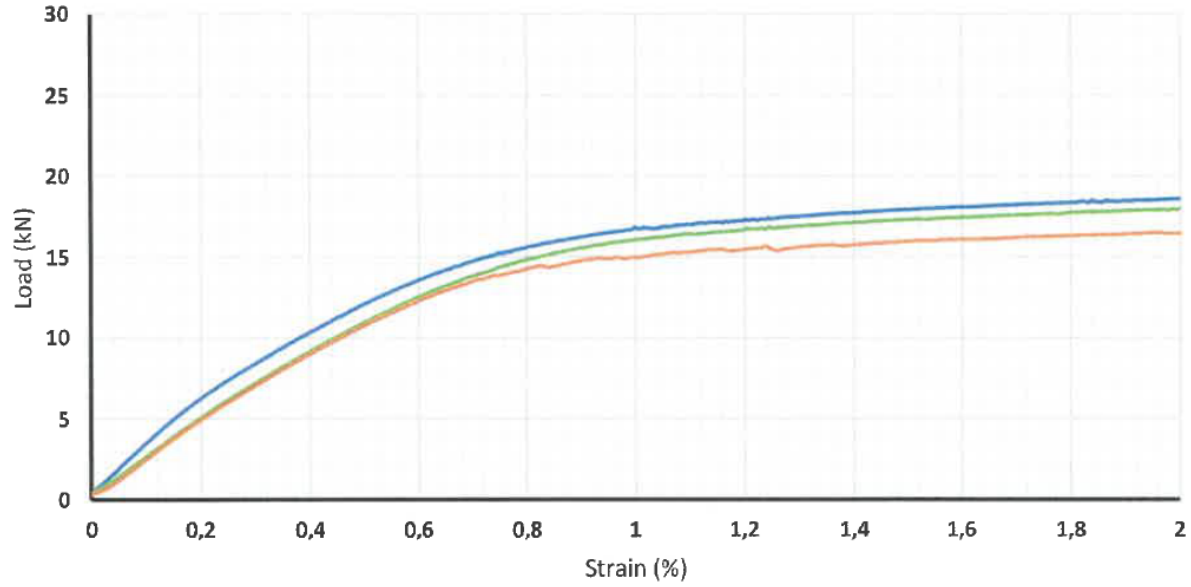

Figure 24: As-build Load-Strain curve, vertical direction.

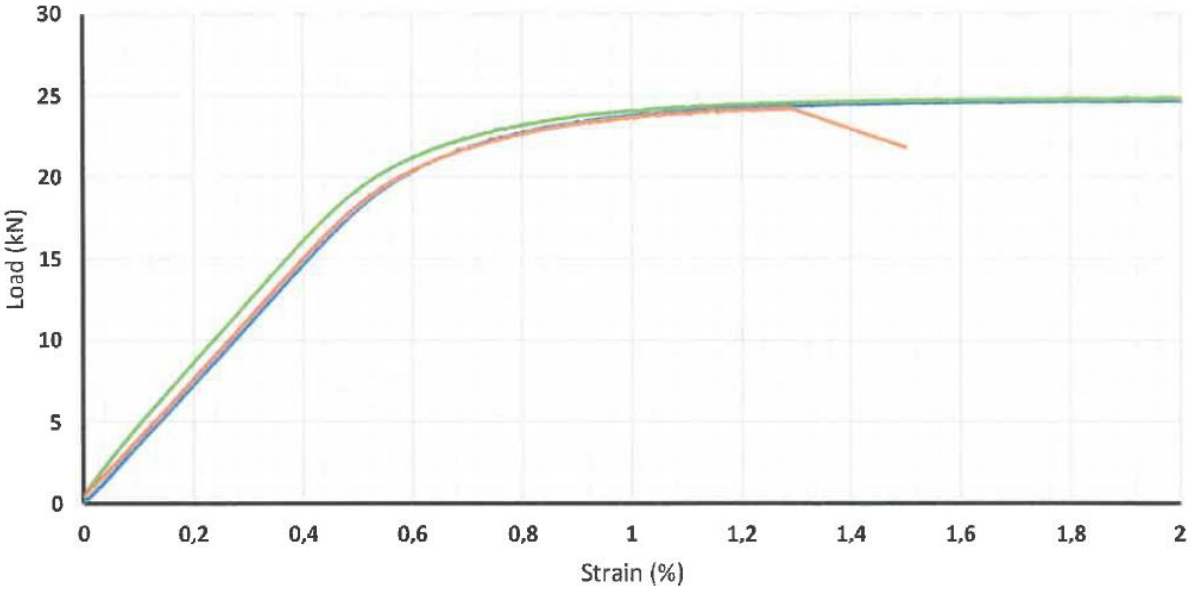

Figure 25: H900 Load-Strain curve, vertical direction.

- *Directional dependence is removed as a result of HT including solution annealing.* The origin for this could be the loss of directionality in the microstructure which has been observed. Samples that did not undergo a solution heat treatment maintain a directional microstructure. However, the directional dependence of this material has not been investigated by means of tensile test specimens. It is therefore not certain that the directionality of the microstructure is the core mechanism. It is also possible that the precipitation of nanosized particles removes the directional dependence. These particles are the main strengthening mechanism and appear evenly spaced within the grains and in all directions. If these particles govern the mechanical properties, and not the presence of grain or other boundaries, than it can be expected that no directional dependence is observed.

4.5.2 Does performing a solution annealing treatment influence the properties after HT?

The cube specimens indicate that the samples that did not undergo a solution annealing heat treatment have a higher hardness, irrespective of the used process parameters (high or low power setting).

Both the yield strength and tensile strength of the H900 samples in Batch 2 (lower power setting, no solution annealing) are around 200MPa lower as compared to the H900 samples in Batch 1. On the other hand, the hardness measured on the ends of the tensile samples are higher for Batch 2, where no solution annealing is performed (+20 HV10, same density). This agrees well with the hardness results from the cube specimens, where the hardness of the solution annealed samples is in the range of 30 HV10 lower. From these results one can conclude that not performing the solution annealing treatment increases the hardness, but has a negative effect on the tensile properties.
The samples from both batches have virtually the same density, however they have a very different microstructure. The solution annealed samples exhibit a more uniform structure of tempered martensite, with much smaller grain sizes. The tensile test results also indicate that the solution annealed H900 samples have a somewhat higher ductility (elongation 7.5% vs. 4%). A limited amount of necking can be seen on the solution annealed samples, while the non-solution annealed samples appear to have a completely brittle fracture surface.
Based on these observations, it may be deduced that omitting solution annealing increases the potential for hardening by precipitation of nanoparticles to some extent (which is in direct contradiction to the results from [5], see section 2.3.2.). A possible explanation for this could be that the as-build state, due to the rapid quenching, already contains a very homogeneous solid solution of the precipitating elements and thus the as-build material contains the full potential for precipitation hardening. Cooling after the solution treatment is slower, possibly already resulting in the formation of some coarser precipitates. The higher temperature also results in destruction of the very fine cellular microstructure observed by SEM (still observed in the non-solution treated samples, not in the solution treated samples). Although these mechanisms may intuitively help to explain the higher observed hardness in the non-solution annealed H900 samples, the physical mechanism responsible has not been studied further and could be a topic of interest for future academic research.
In addition, the coarse grain structure of the non-solution annealed samples may reduce ductility. In the presence of defects, a hard but brittle structure will tend to have reduced tensile properties (as is well known for typical ceramic materials). In contrast, the fine grain structure in the solution annealed samples can allow for a higher ductility and possibly crack branching and blunting. As a result, although the hardness is (slightly) lower, the solution annealed sample has improved tensile properties.

The above discussion also suggests that faster cooling after annealing might lead to both an increased hardness and improved tensile properties. This is further supported by [14], where it is shown that premature Cu-precipitation takes place during slow cooling (0.01-10 K/s) in the temperature range from 1000°C to 680°C. The critical cooling rate to suppress this premature precipitation is shown to be 10–20 K/s for L-PBF steel. The cooling rate for the current annealing was on the order of 0.17 K/s in the temperature range of interest. For conventional material, the critical cooling rate found in [14] was 1K/s. It was not investigated whether the difference between conventional and L-PBF material was due to a difference in composition, mainly Cu content, or structure.

4.5.3 How do the properties after HT compare to AB, and conventional material?

- Spread in properties as a function of position on build plate does not change significantly as a result of HT. Only clear conclusion that can be drawn is that the tensile strength and elongation spread is reduced after H1150.
- *Highest strength and lowest elongation is obtained from the H900 heat treatment*, which is as expected. The lower treatment temperature results in a larger driving force for nucleation and a larger number of smaller precipitates. (For the impact of solution annealing, see above.)
- *The H1150 treated material has a lower yield strength than the as-built material, but exhibits significant strain hardening* in the first 1.5-2% strain after yielding. In contrast, The amount of strain hardening for both the as-built and H900 samples is limited. The tensile strength of the H1150 material exceeds that of the as-built material, but stays well below that of the H900 material.

- *Compared to the conventional material*, the 3D printed material has a lower yield strength (-100MPa) and lower tensile strength (-100MPa) for the H900 treatment. After the H1150 treatment, the yield strength is also significantly lower (-200MPa), but the tensile strength is as expected. The higher amount of strain hardening and elongation for the 3D printed material after H1150 explains why the tensile strength of the conventional material is reached while the yield strength is lower.
- *Within the current study, it seems that the AB condition has slightly better properties as compared to the H1150 condition.*

		R_P [MPA]	R_M [MPA]	ε_m [%]	HRC
CONDITION A	Conventional (ATI)	760	1030	8	33
AS-BUILD	SLM Solutions	572	832	31	<20(1)
	3D Systems 17-4PH(2)	830	1100	19	32
	Current results(2)	727	988	15.7	34,6(4)
H900	Conventional (ATI)	1240	1340	10	43
	Concept Laser	1250	1350	5	43-46
	3D Systems 17-4PH(2)	1260	1380	12	40
	Current results(2)(3)	1160	1265	7.5	42,5(4)
H1150	Conventional (ATI)	860	1000	10	31
	Concept Laser	820	900	13	31-35
	3D Systems 17-4PH(2)	1020	1080	16	35
	Current results(2)	656	978	16.2	30,5(4)

(1) Conversion from 221 HV10 using hardness conversion table
(2) Data taken for the Z-direction
(3) HT including solution annealing
(4) Converted from HV10 using hardness conversion table

4.5.4 Does a change in process parameters from high power and scan speed to low power and scan speed influence the properties?

The machined AB (no HT) samples produced with lower power settings (batch 2) have slightly higher yield strength and lower tensile strength as compared to those produced with high power settings (batch 1), and significantly reduced elongation. AB (no HT) samples from batch 2 also have a lower hardness.

The density of the machined samples from batch 2 could not be measured, however from the density measured on the AB surface samples, and the observation that the variation within similar builds of batch 1 is minimal, it can be safely deduced that a change in density will not be the origin of these observations. In addition, the results from the cube samples confirm that the samples build with a lower power and scan speed have a lower as-build (no HT) hardness. That would mean that the observed change in tensile properties is indeed linked to a change in process parameters.

The high power samples show a very stable columnar growth, while the microstructure of the low power samples is much more chaotic. Based on visual appearance, one could also argue that the amount of retained austenite is somewhat higher in the low power samples. The latter might explain a lower hardness, but on the other hand, because the material has a good ductility, a higher yield stress would also be expected. No explanation for this discrepancy between hardness and yield stress has currently been found.

The machined H900 samples from batch 2 have significantly lower Rp, Rm and elongation as compared to batch 1. Due to change in process parameters? Due to change in density? Or due to lack of solution annealing?

Also for the H900 samples a change in density doesn't not seem to be the main cause. In addition, it is observed that the hardness of the samples in batch 2 is higher. The fracture surface of the H900

samples is indicative for brittle fracture. This could explain why a higher hardness is linked to lower tensile properties. From the tensile test data, it cannot be concluded with certainty whether the change in properties results from the change in heat treatment or from a change in process parameters. However, the hardness measurements indicate that the hardness is different depending on whether or not solution annealing is applied, within a set of sample printed with identical process parameters. This can be an indication that it is the heat treatment that has the major effect and overshadows the effect from the change in process parameters. See 4.5.2 for a discussion on the influence of the solution heat treatment.

4.5.5 Does the hardness correlate well to the tensile properties? And can it thus be used as a simple and fast tool for parameter optimization.

The hardness of non-solution annealed samples (batch 2) is higher as compared to solution annealed samples (batch 1), while the tensile properties are significantly lower (see question 2). On the other hand, the results from the cube samples show that the hardness correlated to the density within a set of similar samples. This is also illustrated by the density and hardness measured on the ends of non-solution annealed H900 tensile samples in the table below.

Sample no.	Hardness [HV10]	Density [%]
1	369	95.88
2	432	98.69
3	445	98.69

Table 7: Results hardness measurement performed on the ends of tensile samples from Batch 2, non-solution annealed H900, as-build surface

From the above, it can be concluded that the hardness can be used as an indicator for density, within a set of samples having received the same post treatment and build with similar print parameters. But that it cannot be used as an indicator for the tensile properties when comparing different types of heat treatment and process parameters. This is confirmed by the discussion in 4.5.2.
These conclusions also show that hardness measurement is perhaps not the perfect tool for parameter optimisation. It is correlated to density, but density is also quick to measure. In addition, the hardness is only lightly correlated to the process parameters. More importantly, for most applications the tensile properties are the critical parameters, and the hardness does not show a good correlation to the tensile properties.

4.5.6 Does the surface condition influence the tensile properties?

Yield strength is lower for the AB NNS samples, this could be related to an early onset of plasticity at stress raisers at the surface. This should result in a more gradual transition from elastic to plastic as compared to the machined samples, which is indeed confirmed by the load-strain curves. The ultimate tensile strength for machined and NNS AB samples is the same. This illustrates that, if sufficient plastic deformation and work hardening is possible, the initial yielding at local stress raisers does not result in early fracture because the plastic zone can spread throughout the sample cross section.

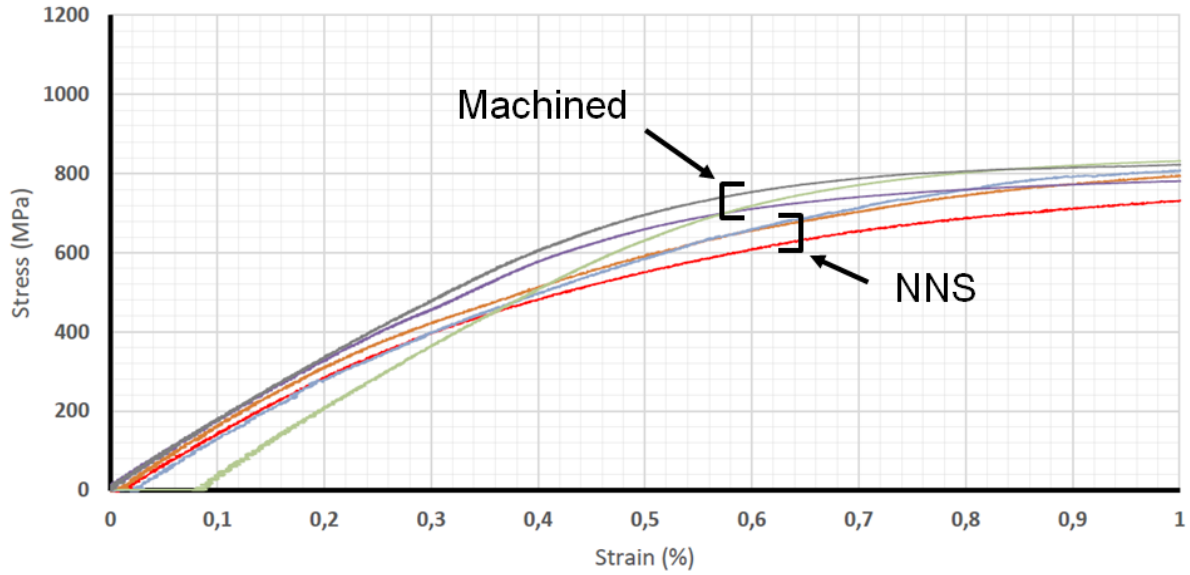

Figure 26: Stress-strain curves for as-build, machined and NNS tensile specimens.

The NNS samples do however exhibit a much larger spread in elongation at fracture. A possible interpretation could be the following: Although the plastic deformation can spread from a local stress raiser throughout the entire cross section, resulting in the same tensile strength for NNS as machined samples, the potential for the plastic zone to spread along the length of the sample and cause necking depends on the distribution of stress raisers around the initial plastic zone. If the initial stress raiser is very strong compared to other stress raisers around it, the work hardening will not be sufficient to activate plasticity along the length of the sample. If that is the case, samples with small elongation should have a lower macroscopic yield stress (strong stress concentrator). In the small data set we have, this appears to be the case, but there is insufficient data to proof this point.
After precipitation hardening (H900), the yield strength of the machined samples is increase, but the elongation at fracture reduced significantly. The precipitation hardened NNS samples failed in a brittle manner, and most samples also failed at a low macroscopic load. The reduced potential for plastic deformation and work hardening means that the tips of cracks initiating at surface stress concentrators, cannot be blunted sufficiently, resulting in early failure of the NNS samples. For the one NNS sample which did not fail early, the properties are comparable to the machined samples (R_p and R_m, ε_m not measured – fracture outside strain gauge). This illustrates that the intrinsic material properties are not affected, but that the properties of the NSS samples show a strong probabilistic spread.

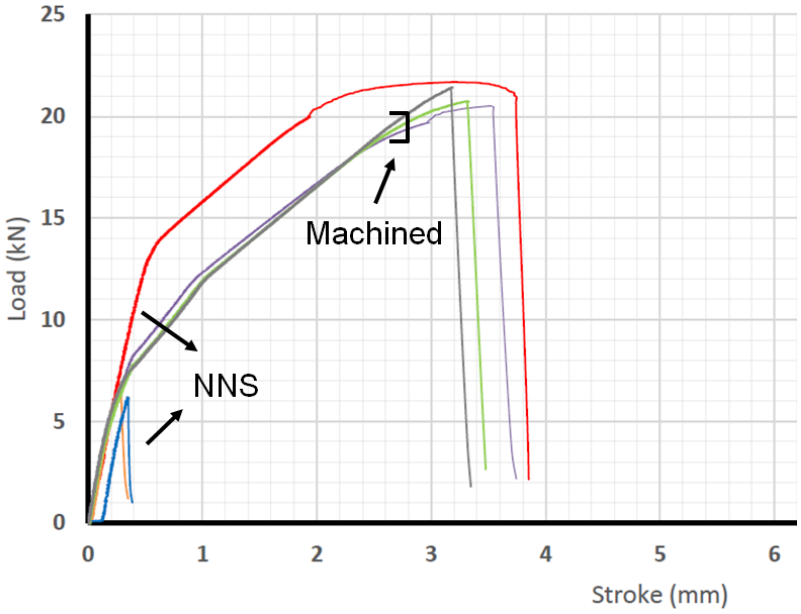

Figure 27: Load-stroke curve for H900 non solution annealed samples.

Above, the stroke curve is shown for the H900 samples (no sol. HT) to illustrate the spread in elongation for the NNS samples. Below, the stress-strain curve is shown, but for two of the NNS samples, elongation and fracture occurred outside the strain gauge.

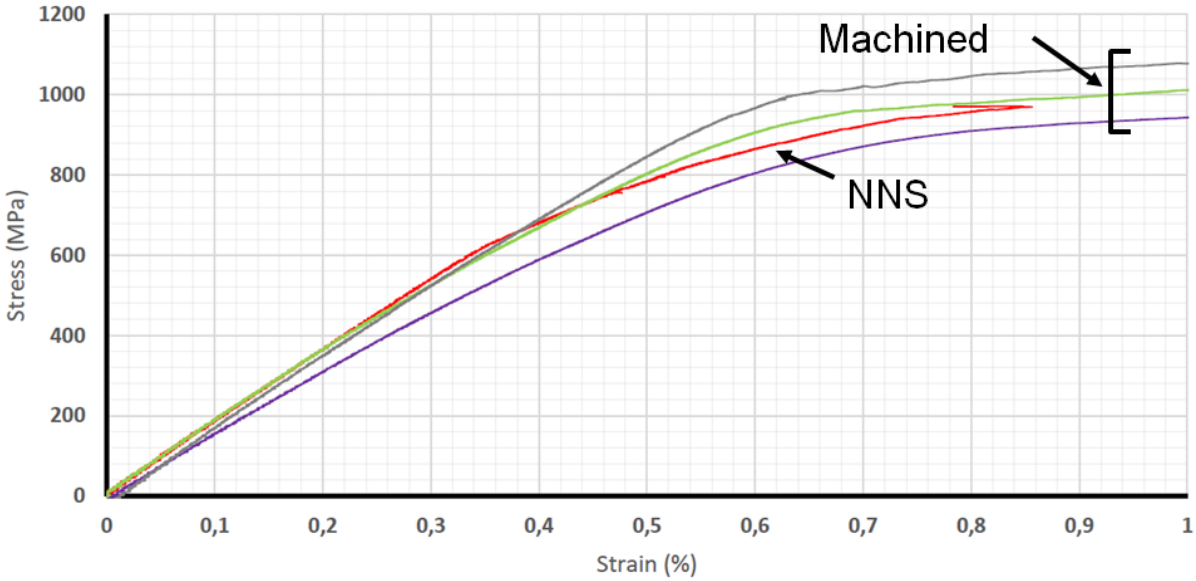

Figure 28: Stress-strain curve for H900 non solution annealed samples. NNS sample broke outside the strain gauge, strain where the curve stops is therefore not necessarily equal to ε_m.

In conclusion, it can be said that surface roughness of NNS parts clearly has a negative impact on the performance of high strength/low elongation materials. The impact on materials allowing a larger amount of plastic deformation such as the AB samples is smaller, however the yield strength is still reduced significantly. Post-processing of the surface to reduce the roughness is advised. As a minimum precaution, cleaning by sand-blasting is suggested, although in the current investigation the effects of sand blasting have not been investigated.

There appears to be an inverse correlation between hardness and yield strength, although the amount of data available is insufficient to draw hard conclusions on this. Should there indeed be an inverse correlation, more testing is required to elucidate the mechanism responsible.

5 Surface post-processing of SLM 17-4PH

For the results of surface post-processing the reader is referred to the complementary information in the document 'Surface finishing of L-PBF and LMD parts' on the project webpage[2].

6 Printing of demonstrator parts

A demonstrator part was developed and printed using 17-4PH steel. As a generalised demonstrator, a type of rotor was designed, as shown in Figure 30. The total height of the printed rotor is 225mm. For more information on the demonstrator, it's design and an economic evaluation, see the complementary information in the document 'L-PBF vs. LMD - Case study using a Generalised Rotor' on the project webpage[2]. Here, a few points of attention, encountered while printing are described:

1. ***Importance of powder weight and layer thickness:*** the machine used for printing had previously mainly been used for aluminium powders. Upon printing of the 17-4PH steel, the powder wiper came lose due to the powder being to heavy. The wiper had to be fixed more securely to avoid this problem.
2. ***Importance of part orientation:***
    1. *Avoid surface orientation close to the limit:* At an inclination of 45° from the vertical direction, an unacceptably rough down facing surface was observed.
    2. *Avoid large and long horizontal sections:* When printing the rotor in a completely vertical direction, the section to print changes radically when coming from shaft to the rotor itself. As a result a large layer has to be printed on the support structure, which leads to a rougher printed layer. It proved more difficult to spread powder evenly over this rough layer, resulting in a build failure.
    3. *Influence on thermal dissipation:* Higher tilts lead to a decreased heat removal through the part itself. Supports were added to compensate for this, based on experience with Ti, but this proved insufficient. More supports might have worked, but here the choice was made to work with smaller inclination to avoid a rough down facing surface. Overheating lead to defects near the top of the part (instability of melt pool/surface deformation).
3. ***Necessity to heat treat:*** In some builds (depending on part orientation), the part supports came loose from the build plate, clearly indicating the presence of residual stresses. In order to make sure that no deformation occurs when cutting parts of this size from their build plate, it is advised to perform a stress relief heat treatment prior to removal from the build plate.
4. ***Importance of sieving under atmosphere:*** At the location of the discoloration, recycled powder was fed into the machine. After noticing the discoloration, it was found that there was a problem with the protective gas enclosure during sieving, leading to an increased amount of oxidation. Tensile samples with a similar discoloration were found, but failure did not occur at that location on the sample.
5. ***Powder removal:*** The design is not ideal when it comes to removal of powder from inside the rotor.

[2] https://www.sirris.be/inside-metal-additive-manufacturing

Figure 29: Failed build of a demonstrator part. Following defects can be observed: (1) an unacceptably rough down facing surface, (2) coming loose of support structures and (3) near the top faults related to overheating.

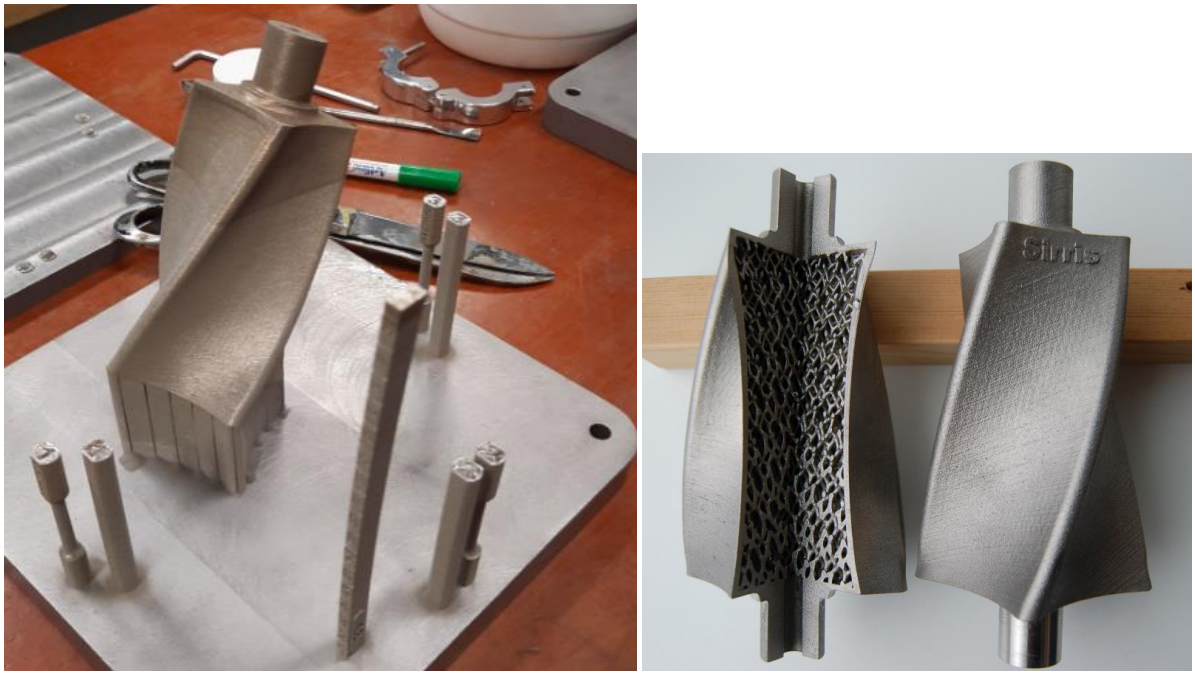

Figure 30: Left: Rotor printed at 100% scale, still attached to build plate. A discoloration is seen around ¼ from the top. Right: Finished demonstrator parts printed at a scale of 75%.

7 Conclusions and Lessons learned

Summarizing the results and discussion presented in this report, the following lessons were learned:

- ***Print parameters***
  - While a clear influence of print parameters both on AB microstructure and properties has been found, overall the impact of changing print parameters on the mechanical properties (both hardness and tensile) is negligible from an industrial point of view.
  - In addition, the influence of print parameters is largely erased after applying a heat treatment (even without solution annealing).
  - **Process parameter optimisation *for heat-treatable materials* should therefore focus on optimising density first and productivity (print speed) second. The same procedure was followed for 17-4PH in [15].** (The is not necessarily true for non-heat-treatable materials, where the ab-build microstructure is maintained in the final part.)
  - Using Energy Density as a parameter to characterise the print process doesn't capture all the influences required for complete optimisation, i.e. there is not a single value for energy density where the highest density is observed. However, the energy density can be used to determine a subset of parameter space within which the highest material densities can be found and where further optimisation should focus on.
  - Hardness [HV10] is correlated to density up to densities of densities of around 99%. Within this study, hardness is however not correlated to the tensile properties and is not a good tool for print parameter optimisation.
- ***Process stability***
  - Gas flow over the powder bed has an important effect on process stability and achievable material density. Gas flow is related to both hardware (e.g. air filters) and a number of parameters such as speed of pumps, closing angle of valves, balance between back and front valves, etc. Experimentation is required to find the best possible settings and sometimes a compromise has to be made between material properties and for example dust collecting on the machine window.
- ***Anisotropy***
  - A columnar grain structure is observed, leading to some anisotropy in the mechanical properties. Although the numerical differences between X-Y and Z direction are smaller than 10%, an important difference is that the elastic-plastic transition is much more gradual along the Z-direction.
  - Solution annealing completely removes the columnar grain structure and anisotropy in the mechanical properties.
- ***Heat treatment***
  - The as-build material contains the full potential for precipitation hardening, meaning that no solution annealing treatment is required in order to make precipitation hardening possible.
  - Solution annealing results in a uniform structure of tempered martensite, while the microstructure of non-solution annealed samples appears unchanged as compared to the AB structure.
  - Within the heat treatments as applied in this study, omitting solution annealing increases the potential for hardening by precipitation of nanoparticles to some extent, but results in a reduction of the tensile properties.
  - Sufficiently fast cooling after annealing may be critical in order to prevent pre-mature and undesired precipitation (leading to larger precipitates with less strengthening effect).
  - The choice of heat treatment has a major impact on the properties of the 3D printed 17-4PH steel. By tailoring the heat treatment, the material properties can be tailored,

with the optimal heat treatment for the 3D printed steel not necessarily being the same as for the conventional steel.
    - **The heat treatment therefore needs to be carefully considered as a critical step in the process chain.** And a good control of the heat treatment is thus required, even if it is only meant to reduce residual stresses, as the properties of the material may be influenced even when this was not the intention.
    - Based only on tensile properties and hardness, the AB material seems to have slightly better properties as compared to the H11150. Depending on the application, it is therefore not a-prior certain that a heat treatment is compulsory. (Important remark here is that the residual stresses in the AB material were not considered as a possible source of deformation and failure.)
- ***Surface condition***
    - The condition (roughness) of the surface has a major influence on the tensile properties of the harder and more brittle H900 treated 17-4PH steel. In comparison, the impact of the surface condition on the more ductile as-build 17-4PH steel is limited.
- ***Printing of demonstrator***
    - The most important lessons learned from printing of the demonstrator can be found in chapter 6.

Bibliography

[1] T. DebRoy et al., Additive manufacturing of metallic components – Process, structure and properties, Progress in Materials Science 92 (2018) 112–224
[2] L. Zai, Laser Powder Bed Fusion of Precipitation-Hardened Martensitic Stainless Steels: A Review, Metals 10 (2020) 255
[3] Y. Sun, Effect of heat treatments on microstructural evolution of additively manufactured and wrought 17-4PH stainless steel, Materials and Design 156 (2018) 429–440
[4] P. Bajaj, Steels in additive manufacturing: A review of their microstructure and properties, Materials Science & Engineering A 772 (2020) 138633
[5] M. Mahmoudi, Mechanical properties and microstructural characterization of selective laser melted 17-4 PH stainless steel, Rapid Prototyping Journal 23/2 (2017) 280–294
[6] H. Gu, Influences of energy density on porosity and microstructure of selective laser melted 17-4PH stainless steel, Proceedings of Solid Freeform Fabrication Symposium (2013) 474-479
[7] H.K. Rafi, Microstructure and mechanical behavior of 17-4 precipitation hardenable steel processed by selective laser melting, Journal of Materials Engineering and Performance, 23/12 (2014) 4421-4428
[8] S. Cheruvathur, Additive Manufacturing of 17-4 PH Stainless Steel: Post-processing Heat Treatment to Achieve Uniform Reproducible Microstructure, The Minerals Metals & Materials Society, 68/3 (2015) 930-942
[9] P. Ferro, A modified volumetric energy density–based approach for porosity assessment in additive manufacturing process design, The International Journal of Advanced Manufacturing Technology 110 (2020) 1911–1921
[10] B. Piotr, The Kinetics of phase transformations during continuous heating from as-quenched state of 17-4PH Steel, Metal 2015, June 3rd-5th, Bruno, Czech Republic, 2015
[11] Z. Wang, Nano-precipitates evolution and their effects on mechanical properties of 17-4 precipitation-hardening stainless steel, Acta Materialia, 156 (2018) 158-171
[12] G. Jacob, Prediction of Solidification Phases in Cr-Ni Stainless Steel Alloys Manufactured by Laser Based Powder Bed Fusion Process, NIST Advanced Manufacturing Series 100-14, 2018
[13] T. Starr, Controlling Phase Composition in Selective Laser Melted Stainless Steels, International Solid Freeform Fabrication Symposium, University of Texas, Austin (2012) 439-446.
[14] C. Rowolt, Dissolution and precipitation of Cu-rich phases during heating and cooling of steel 17-4PH, J Mater Sci 55 (2020) 13244–13257
[15] Additive Manufacturing of highly-stressed components in hardened martensitic stainless steel, MAM Magazine, Online, 22/02/2021, https://www.metal-am.com/additive-manufacturing-of-highly-stressed-components-in-hardened-martensitic-stainless-steel/
[16] ASM Handbook Volume 9: Metallography and Microstructures

Appendix A – Typical wrought 17-4PH microstructure, from [8]

The figure below, copied from [8], shows the typical martensitic microstructure of as-received wrought 17-4 steel having a hardness of 322 ± 10 Vicker's hardness (VH). δ-ferrite stringers are observed likely aligned along the rolling direction (formed during initial solidification). The x-ray diffraction (XRD) pattern has Bragg reflections corresponding to only BCC/martensite (b). After subjecting to condition A heat treatment, the α' lath structure is retained (c and d), and the material has a hardness of 299 ± 11 VH. Examining the microstructure at a higher magnification reveals the presence of fine precipitates throughout the matrix (e). Based on x-ray mapping (f), these precipitates are presumed to be Nb-rich carbides.

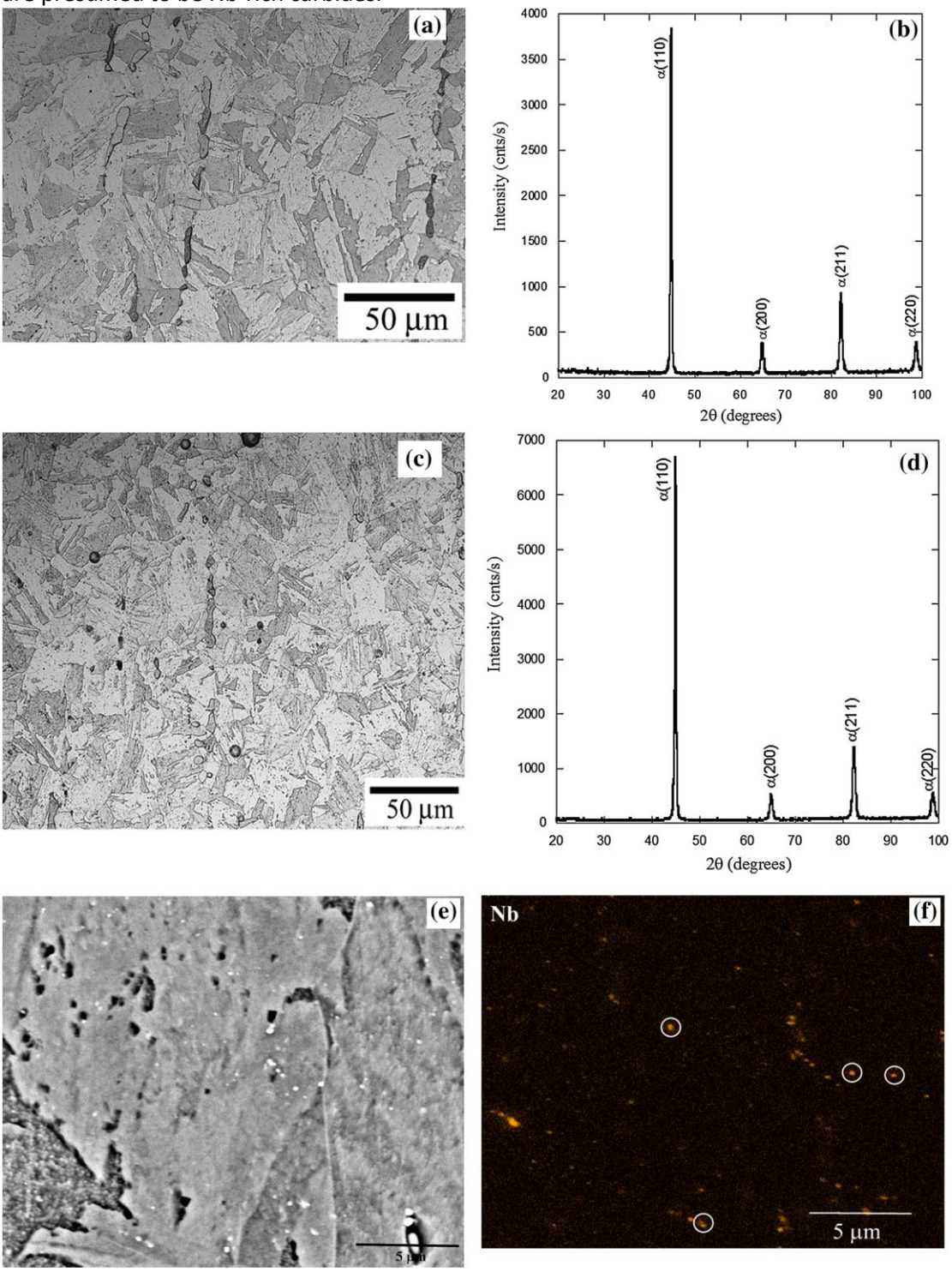

Appendix B – 17-4PH phase diagrams, from [8]

Composition of 17-4PH indicated with the vertical black dotted line.